Tryptophan-Kynurenine Metabolic Remodeling and Complementary Pathways in Kynurenine Aminotransferase II Knockout Mice with Relevance to Neuropsychiatric Phenotypes

Ágnes Szabó

Ph.D. Thesis

University of Szeged

Albert Szent-Györgyi Medical School

Doctoral School of Clinical Medicine

Department of Neurology

Tryptophan-Kynurenine Metabolic Remodeling and Complementary Pathways in Kynurenine Aminotransferase II Knockout Mice with Relevance to Neuropsychiatric Phenotypes

Ágnes Szabó

Ph.D. Thesis

Supervisor(s):

László Vécsei, M.D., Ph.D., D.Sc.

Masaru Tanaka, M.D., Ph.D.

Szeged

2026

Original Publication directly related to the Ph.D. thesis:

I. **Szabó Á.,** Galla Zs., Spekker E., Szűcs M., Martos D., Takeda K., Ozaki K., Inoue H., Yamamoto S., Toldi J., Ono E., Vécsei L., Tanaka M. *Oxidative and Excitatory Neurotoxic Stresses in CRISPR/Cas9-Induced Kynurenine Aminotransferase Knockout Mice: A Novel Model for Despair-Based Depression and Post-Traumatic Stress Disorder.* **Frontiers in Bioscience Landmark** 2025, 30(1): 25706. doi: 10.31083/FBL25706 (**original paper, Q2, IF: 3.100 (2025))**

II. **Szabó Á.,** Galla Zs., Spekker E., Martos D., Szűcs M., Fejes-Szabó A., Fehér Á., Takeda K., Ozaki K., Inoue H., Yamamoto S., Monostori P., Toldi J., Ono E., Vécsei L., Tanaka M. *Behavioral Balance in Tryptophan Turmoil: Regional Metabolic Rewiring in Kynurenine Aminotransferase II Knockout Mice.* **Cells** 2025, 14, 1711. doi: 10.3390/cells14211711 (**original paper, Q1, IF: 5.200 (2025))**

Quartile ranking of the publication directly related to the thesis: 1 Q1 + 1 Q2
Cumulative impact factor of the publications directly related to the thesis: 8.300

Publications not directly related to the Ph.D. thesis:

I. Tanaka M., **Szabó Á.,** Lőrinczi B., Szatmári I., Fülöp F., Vécsei L. Antidepressant-like Effects of Kynurenic Acid Analogues. **Proceedings of 1st International Electronic Conference on Biomedicine** 2021, 10301, 8 p. doi: 10.3390/ECB2021-10301

II. Tanaka M., Tóth F., Polyák H., **Szabó Á.,** Mándi Y., Vécsei L. Immune Influencers in Action: Metabolites and Enzymes of the Tryptophan-Kynurenine Metabolic Pathway. **Biomedicines** 2021, 9, 734. doi: 10.3390/biomedicines9070734 **(Q1, IF: 4.757 (2021))**

III. Tanaka M., Török N., Tóth F., **Szabó Á.,** Vécsei L. *Co-Players in Chronic Pain: Neuroinflammation and the Tryptophan-Kynurenine Metabolic Pathway.* **Biomedicines** 2021, 9, 897. doi: 10.3390/biomedicines9080897 **(Q1, IF: 4.757 (2021))**

IV. Spekker E., Tanaka M., **Szabó Á.,** Vécsei L. *Neurogenic Inflammation: The Participant in Migraine and Recent Advancements in Translational Research.* **Biomedicines** 2021, 10, 76. doi: 10.3390/biomedicines10010076 **(Q1, IF: 4.757 (2021))**

V. Tanaka M., Spekker E., **Szabó Á.,** Polyák H., Vécsei L. *Modelling the neurodevelopmental pathogenesis in neuropsychiatric disorders. Bioactive kynurenines and their analogues as neuroprotective agents—in celebration of 80th birthday of Professor Peter Riederer.* **Journal of Neural Transmission** 2022. doi: 10.1007/s00702-022-02513-5 **(Q2, IF: 3.300 (2022))**

VI. Tanaka M., **Szabó Á.,** Spekker E., Polyák H., Tóth F., Vécsei L. *Mitochondrial Impairment: A Common Motif in Neuropsychiatric Presentation? The Link to the Tryptophan–Kynurenine Metabolic System.* **Cells** 2022, 11, 2607. doi: 10.3390/cells11162607 **(Q1, IF: 6.000 (2022))**

VII. Tanaka M., **Szabó Á.,** Vécsei L. *Integrating Armchair, Bench, and Bedside Research for Behavioral Neurology and Neuropsychiatry: Editorial.* **Biomedicines** 2022, 10, 2999. doi: 10.3390/biomedicines10122999 **(Q1, IF: 4.700 (2022))**

VIII. Tajti J., Szok D., Csáti A., **Szabó Á.,** Tanaka M., Vécsei L. *Exploring Novel Therapeutic Targets in the Common Pathogenic Factors in Migraine and Neuropathic Pain.* **International Journal of Molecular Sciences** 2023, 24, 4114. doi: 10.3390/ijms24044114 **(Q1, IF: 4.900 (2023))**

IX. Polyák H., Galla Zs., Nánási N., Cseh E.K., Rajda C., Veres G., Spekker E., **Szabó Á.,** Klivényi P., Tanaka M., Vécsei L. *The Tryptophan-Kynurenine Metabolic System Is Suppressed in Cuprizone-Induced Model of Demyelination Simulating Progressive Multiple Sclerosis.* **Biomedicines** 2023, 11, 945. doi: 10.3390/biomedicines11030945 **(Q1, IF: 3.900 (2023))**

X. Tanaka M., **Szabó Á.,** Vécsei L. *Preclinical modeling in depression and anxiety: Current challenges and future research directions.* **Advances in Clinical and Experimental Medicine** 2023, 32(5). doi: 10.17219/acem/165944 **(Q2, IF: 2.100 (2023))**

XI. Tanaka M., **Szabó Á.,** Körtési T., Szok D., Tajti J., Vécsei L. *From CGRP to PACAP, VIP, and Beyond: Unraveling the Next Chapters in Migraine Treatment.* **Cells** 2023, 12, 2649. doi: 10.3390/cells12222649 **(Q1, IF: 5.100 (2023))**

XII. Tanaka M., **Szabó Á.,** Vécsei L., Giménez-Llort L. *Emerging Translational Research in Neurological and Psychiatric Diseases: From In Vitro to In Vivo Models.* **International Journal of Molecular Sciences** 2023, 24, 15739.doi: 10.3390/ijms242115739 **(Q1, IF: 4.900 (2023))**

XIII. Tanaka M., **Szabó Á.,** Vécsei L. *Redefining Roles: A Paradigm Shift in Tryptophan–Kynurenine Metabolism for Innovative Clinical Applications.* **International Journal of Molecular Sciences** 2024, 25, 12767. doi: 10.3390/ijms252312767 **(Q1, IF: 4.900 (2024))**

XIV. Juhász L., Spisák K., Szolnoki B.Zs., Nászai A., **Szabó Á.,** Rutai A., Tallósy Sz.P., Szabó A., Toldi J., Tanaka M., Takeda K., Ozaki K., Inoue H., Yamamoto S., Ono E., Boros M., Kaszaki J., Vécsei L. *The Power Struggle: Kynurenine Pathway Enzyme Knockouts and Brain Mitochondrial Respiration.* **Journal of Neurochemistry** 2025, 169:e70075. doi: 10.1111/jnc.70075 **(Q1, IF: 3.700 (2024))**

Quartile ranking of publications not directly related to the thesis: 11 Q1 + 2 Q2
Cumulative impact factor of publications not directly related to the thesis: 57.771
Total quartile ranking: 12 Q1 + 3 Q2
Total impact factor: 66.071

Posters directly related to the thesis:

I. **Szabó Á.,** Spekker E., Fejes-Szabó A., Nánási N., Toldi J., Tanaka M., Ono E., Vécsei L. *Low Plasma Kynurenic Acid Sustains Normal Cognitive Maturation.* **9th Congress of the European Academy of Neurology;** July 01-04, 2023; Budapest, Hungary

II. **Szabó Á.,** Galla Zs., Spekker E., Szűcs M., Martos D., Takeda K., Ozaki K., Inoue H., Yamamoto S., Toldi J., Ono E., Tanaka M., László V. *Unraveling the Impact on Catecholamines and Cognitive Functions in Novel Kynurenine Aminotransferase*

Knockout Mice. **16th Congress of the International Society for Tryptophan Research (ISTRY);** April 24-26, 2024; Jena, Germany

Posters not directly related to the thesis:

I. Tanaka M., **Szabó Á.,** Lőrinczi B., Szatmári I., Fülöp F., Vécsei L. *Antidepressant-like Effects of Kynurenic Acid Analogues.* **The 1st International Electronic Conference on Biomedicine;** 01-26 June, 2021; online

II. Juhász L., Nászai A., **Szabó Á.,** Spekker E., Tallósy Sz.P., Szolnoki B., Rutai A., Tanaka M., Ono E., Toldi J., Vécsei L., Boros M., Kaszaki J. *Az elektrontranszportlánc működési zavarai kinurenin aminotranszferáz enzimhiányos egerekben.* **Magyar Élettani Társaság (MÉT) LXXXIV. Vándorgyűlése;** 13-16 July, 2022; Budapest, Hungary

III. **Szabó Á.,** Tanaka M., Spekker E., Toldi J., Ono E., Vécsei L. *Kynurenine Aminotransferase II Knockout Mice Mimic Depression with Psychomotor Retardation.* **The 2nd International Electronic Conference on Biomedicines;** 01-31 March, 2023; online

IV. **Szabó Á.,** Spekker E., Fejes-Szabó A., Tanaka M., Toldi J., Ono E., Vécsei L. *Kynurenine Aminotransferase II Knockout Mice Show Increased Pain Sensitivity.* **13th Congress of the European Pain Federation EFIC®;** 20-22 September, 2023; Budapest, Hungary

V. Juhász L., Spisák K., Szolnoki B.Zs., Nászai A., **Szabó Á.,** Rutai A., Tallósy Sz.P., Szabó A., Toldi J., Tanaka M., Takeda K., Ozaki K., Inoue H., Yamamoto S., Ono E., Boros M., Kaszaki J., Vécsei L. *Electron Transport Disturbances in Kynurenine Aminotransferase Knockout Mice.* **22nd European Bioenergetics Conference (EBEC);** 26-31 August, 2024; Innsbruck, Austria

Table of Contents

List of abbreviations

3CT	three chamber test
3-HAA	3-hydroxyanthranilic acid
3-HK	3-hydroxykynurenine
5-HIAA	5-hydroxyindole-3-acetic acid
5-HT	5-hydroxytryptamine/serotonin
5-HTP	5-hydroxytryptophan
AA	anthranilic acid
AhR	aryl hydrocarbon receptor
ANOVA	analysis of variance
CER	cerebellum
CTX	cortex
DA	dopamine
DI	discrimination index
EI	excitotoxicity index
EPM	elevated plus maze
FST	forced swim test
HIPP	hippocampus
IAA	indole-3-acetic acid
IDOs	indoleamine 2,3-dioxygenases
ILA	indole-3-lactic acid
INS	indoxyl sulfate
KAT II	kynurenine aminotransferase II
kat2$^{-/-}$	kynurenine aminotransferase II knockout strain
KATs	kynurenine aminotransferases
KMO	kynurenine 3-monooxygenase
KYN	kynurenine
KYNA	kynurenic acid
KYNU	kynureninase
LDB	light dark box
MBT	Marble burying test
NAD^+	nicotinamide adenine dinucleotide
NORT	novel object recognition test
OBAT	object-based attention test
OFT	open-field test
OSI	oxidative stress index
PAT	passive avoidance test
PI	preference index
PTSD	post-traumatic stress disorder
Q-Q	quantile-quantile
QA	quinolinic acid
QAA	quinaldic acid
SD	standard deviation
STEM	brainstem
STR	striatum
TDO	tryptophan 2,3-dioxygenase
Trp	tryptophan
TST	tail suspension test
Tyr	tyrosine

Summary

Tryptophan (Trp) is an essential amino acid that functions not only as a substrate for protein synthesis but also as a precursor for several metabolically and neurobiologically relevant pathways. In addition to the serotonergic and microbiota-associated indole-pyruvate routes, Trp metabolism interfaces with the tyrosine-dopamine system through shared cofactors and redox-sensitive monoaminergic regulation. The predominant fate of Trp degradation occurs via the kynurenine (KYN) pathway, which generates bioactive metabolites influencing neurotransmission, oxidative balance, immune signaling, and neuronal viability. Dysregulation of these interconnected pathways has been increasingly implicated in neuropsychiatric disorders.

To examine sustained disruption of the KYN pathway regulation, this work characterizes a novel CRISPR/Cas9-generated mouse model carrying a deletion of the *aadat* gene encoding kynurenine aminotransferase II (KAT II), the principal enzyme responsible for brain kynurenic acid (KYNA) synthesis. Genotype verification was performed using TaqMan allelic discrimination assays. In parallel, ultra-high-performance liquid chromatography coupled with tandem mass spectrometry was employed to quantify Trp and its metabolites across central nervous system regions, as well as in plasma and urine. Inferred enzymatic activities and composite indices of oxidative stress and excitotoxicity were calculated to provide functional insight into pathway-level remodeling.

KAT II deficiency induced a pronounced and region-specific reorganization of Trp metabolism across central and peripheral compartments, characterized by reduced KYNA and xanthurenic acid levels, consistently elevated 3-hydroxykynurenine, altered serotonergic, indole-derived, and catecholaminergic fluxes, and increased oxidative and excitotoxic burden. Despite this marked neurochemical imbalance, behavioral alterations were modest and domain-specific, with changes primarily observed in spontaneous exploration and stress-coping paradigms, while cognitive and social performance remained largely preserved.

Overall, these findings indicate that loss of KAT II establishes a state of metabolic vulnerability rather than overt behavioral pathology, providing a translational framework for understanding how Trp metabolic remodeling across interconnected pathways may bias neuropsychiatric susceptibility and inform future therapeutic strategies.

Introduction

Tryptophan metabolism

Tryptophan (Trp) is an essential amino acid whose biological relevance extends beyond its incorporation into proteins, as it serves as a central precursor for several metabolic pathways [1]. These pathways give rise to a diverse array of biologically active metabolites that are critical for maintaining physiological homeostasis. Although the serotonin (5-hydroxytryptamine; 5-HT) pathway represents the most extensively characterized route of Trp metabolism, approximately 95% of Trp is catabolized through the kynurenine (KYN) pathway, leading to the biosynthesis of the energy-carrying cofactor nicotinamide adenine dinucleotide (NAD^+) and multiple bioactive intermediate compounds [2, 3].

The KYN pathway is initiated by a rate-limiting oxidative step catalyzed by tryptophan 2,3-dioxygenase (TDO) and indoleamine 2,3-dioxygenases (IDOs), which convert Trp to N-formyl-L-kynurenine **(Figure 1a**). This unstable intermediate is rapidly hydrolyzed to L-kynurenine (KYN), a central branching metabolite. From this point, KYN enters several downstream routes with distinct functional consequences. Kynurenine 3-monooxygenase (KMO) converts KYN to 3-hydroxykynurenine (3-HK), whereas kynureninase (KYNU) catalyzes the formation of anthranilic acid (AA). Both 3-HK and AA can be further metabolized to 3-hydroxyanthranilic acid (3-HAA), which represents a key metabolic junction. Through oxidative ring cleavage, 3-HAA gives rise to intermediates that are ultimately directed toward picolinic acid or quinolinic acid (QA), the latter serving as a precursor for de novo NAD^+ synthesis [4–7]. In parallel, KYN can be transaminated to kynurenic acid (KYNA) by kynurenine aminotransferases (KATs), which may subsequently be further metabolized to quinaldic acid (QAA) [8, 9]. Among the four identified KAT isoforms (KAT I-IV), KAT II represents the dominant source of KYNA in the brain under physiological conditions, highlighting its pivotal role in controlling flux through this neuroactive arm of the KYN pathway [10].

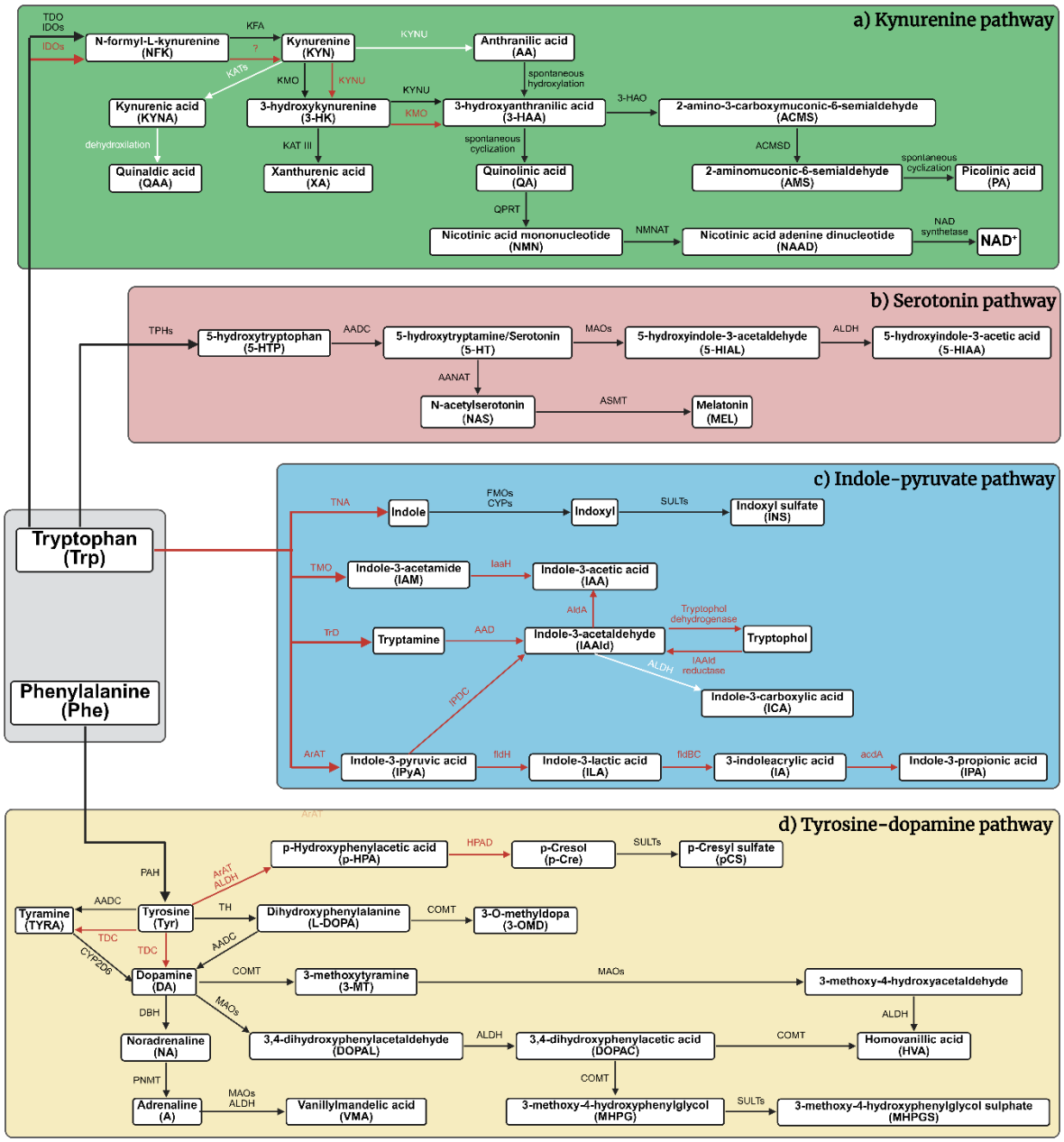

Figure 1. Host- and microbiota-driven tryptophan metabolic pathways, depicting the (a) kynurenine, (b) serotonin, and (c) indole-pyruvate routes, together with their enzymatically linked (d) tyrosine-dopamine pathway [11]. Black arrows indicate host-derived metabolic routes; red arrows denote gut microbiota-driven pathways; white arrows indicate metabolic routes common to both host and microbiota, catalyzed by identical enzymes. 3-HAO, 3-hydroxyanthranilate oxidase; AAD, amino acid decarboxylase; AADC, aromatic L-amino acid decarboxylase; AANAT, arylalkylamine N-acetyltransferase; acdA, acyl-CoA dehydrogenase; ACMSD, amino-*β*-carboxymuconate-semialdehyde-decarboxylase; AldA, indole-3-acetaldehyde dehydrogenase; ALDH, aldehyde dehydrogenase; ArAT, aromatic amino acid

aminotransferase; ASMT, acetylserotonin-O-methyltransferase; COMT, catechol-O-methyltransferase; CYP2D6, cytochrome P450 2D6; CYPs, cytochrome P450 monooxygenases; DBH, dopamine β-hydroxylase; fldBC, phenyllactate dehydratase; fldH, indole-3-pyruvate ferredoxin oxidoreductase; FMOs, flavin-containing monooxygenases; HPAD, 4-hydroxyphenylacetate decarboxylase; IaaH, indole-3-acetamide hydrolase; IDOs, indoleamine 2,3-dioxygenases (IDO1 and IDO2); IPDC, indole-3-pyruvate decarboxylase; KAT III, kynurenine aminotransferase III; KATs, kynurenine aminotransferases (KAT I, II, III, and IV); KFA, kynurenine formamidase; KMO, kynurenine-3-monooxygenase; KYNU, kynureninase; MAOs, monoamine oxidases (MAO-A and MAO-B); NAD^+, nicotinamide adenine dinucleotide; NMNAT, nicotinamide mononucleotide adenylyltransferase; PAH, phenylalanine hydroxylase; PNMT, phenylethanolamine N-methyltransferase; QPRT, quinolinate phosphoribosyl transferase; SULTs, sulfotransferases; TDC, tyrosine decarboxylase; TDO, tryptophan-2,3-dioxygenase; TH, tyrosine hydroxylase; TMO, tryptophan-2-monooxygenase; TNA, tryptophanase; TPHs, tryptophan hydroxylases (TPH1 and TPH2); TrD, tryptophan decarboxylase.

In addition to the KYN pathway, the serotonergic route represents a major but quantitatively minor branch of Trp metabolism, accounting for approximately 2% of total Trp utilization (**Figure 1b**) [12]. Along this pathway, Trp is converted to 5-hydroxytryptophan (5-HTP) and subsequently to 5-HT, a key neuromodulator involved in mood regulation, stress responsiveness, and cognitive processing. 5-HT undergoes tightly regulated turnover, reflecting its dual function as a neurotransmitter and a metabolic intermediate. While a small fraction contributes to melatonin synthesis, the predominant catabolic route yields 5-hydroxyindole-3-acetic acid (5-HIAA), which is commonly used as an index of serotonergic activity [13]. Accordingly, 5-HTP, 5-HT, and 5-HIAA together provide an integrated functional readout of serotonergic pathway dynamics [2, 14, 15].

The indole-pyruvate pathway is gaining increased attention due to its close association with the gut-brain axis and its contribution to approximately 5% of Trp metabolism (**Figure 1c**). This pathway encompasses several microbiota-associated branches that generate bioactive indole derivatives [16]. Key routes include the production of indole and its conversion to indoxyl sulfate (INS), the formation of indole-3-acetic acid (IAA) and related metabolites via monooxygenase-dependent reactions, decarboxylation-derived tryptamine pathways, and aminotransferase-initiated routes yielding indole-3-lactic acid (ILA) and related compounds [17]. These indole metabolites exert immunomodulatory and barrier-protective effects, largely

mediated through aryl hydrocarbon receptor (AhR) signaling, and can indirectly influence central nervous system function through peripheral immune and metabolic mechanisms [18–22].

Trp metabolism further intersects with dopaminergic neurotransmission through its interaction with the tyrosine (Tyr)-dopamine (DA) pathway (**Figure 1d**). Although DA synthesis originates from phenylalanine and Tyr, Trp metabolism may influence this system via shared enzymatic steps, redox sensitivity, and cofactor availability. In particular, tetrahydrobiopterin, an essential cofactor for tyrosine hydroxylase, links Trp metabolism to DA biosynthesis, while its oxidized forms, dihydrobiopterin and biopterin, reflect cofactor turnover and oxidative state [23, 24]. Beyond its role as a neurotransmitter, DA is also a precursor of downstream catecholamines (noradrenaline and adrenaline) involved in stress responses, arousal, and adaptive behavior, linking dopaminergic turnover to broader neuroendocrine and neuropsychiatric regulation [25–27]. Collectively, these interconnected pathways illustrate how perturbations in Trp metabolism can propagate across multiple monoaminergic systems.

Tryptophan Metabolites in Neuropsychiatric Disorders

Beyond its canonical metabolic routes, Trp catabolism constitutes a major regulatory interface through which biochemical signals influence neural, immune, and metabolic processes. The biological activity of Trp-derived metabolites contributes to the modulation of neurotransmission, redox homeostasis, immune signaling, and cellular metabolism, thereby linking peripheral Trp availability to central nervous system function [28, 29]. Among the known degradative pathways, the KYN pathway represents the predominant fate of Trp and generates metabolites with pronounced neurobiological relevance.

Intermediates of the KYN pathway display a wide spectrum of biological activities, encompassing neuroprotective/neurotoxic actions, pro-oxidant/antioxidant properties, as well as potent immunomodulatory effects [3]. Historically, these metabolites have been categorized according to their prevailing functional characteristics, with compounds such as KYNA and AA viewed as neuroprotective, whereas 3-HK, QA, XA, and 3-HAA were associated with oxidative stress and neuronal injury [30]. While this dichotomous framework has been conceptually useful, accumulating evidence indicates that KYN metabolites exhibit pronounced context dependence. Their biological effects are shaped by concentration, cellular origin, and local microenvironment, resulting in a Janus-faced profile in which metabolites may exert protective actions at physiological levels but become detrimental when chronically elevated or

spatially dysregulated. These observations underscore the importance of maintaining metabolic balance within the KYN pathway [31, 32].

Altered Trp metabolism, particularly shifts in the relative production of downstream KYN metabolites, has been documented across a broad range of human diseases. Dysregulation of Trp catabolism has been reported in oncological, autoimmune, neurological, and psychiatric conditions, frequently accompanied by enhanced activation of the KYN pathway [33–39]. Such metabolic reprogramming is often driven by inflammatory or immune-related mechanisms and leads to reduced Trp availability together with changes in the abundance of bioactive KYN intermediates. Increasingly, these alterations are regarded as active contributors to disease-associated functional impairments rather than passive biochemical by-products [39–42].

In neurological disorders, disease-specific patterns of KYN pathway dysregulation have been described, commonly reflecting an imbalance between neuroprotective and neurotoxic branches [43–47]. Similar shifts have been observed in psychiatric conditions, including mood and anxiety disorders, schizophrenia, and neurodevelopmental disorders, where altered KYN metabolite profiles have been linked to changes in neurotransmission, cognitive performance, and emotional regulation. Notably, elevated KYNA levels have been consistently associated with disrupted glutamatergic and cholinergic signaling in schizophrenia, whereas increased flux toward oxidative KYN metabolites has been implicated in affective and stress-related disorders [48–50].

Collectively, these findings point to a robust association between disease-related remodeling of Trp metabolism and functional disturbances of the nervous system, positioning the KYN pathway as a shared biochemical substrate across diverse human pathologies. Despite extensive correlative evidence, however, the causal contribution of KYN pathway dysregulation to disease pathogenesis is not yet fully understood, highlighting the need for experimental models that enable mechanistic dissection of Trp metabolic imbalance.

Novel *kat2*$^{-/-}$ Mice Model

Preclinical research has played a fundamental role in advancing the understanding of neuropsychiatric disorders by enabling the systematic investigation of disease mechanisms under controlled experimental conditions. Through the use of *in vitro* and *in vivo* models, it has become possible to dissect complex molecular pathways, examine their functional consequences, and identify potential therapeutic targets that are difficult to isolate in clinical settings. In particular, animal models have provided indispensable insight into the behavioral,

cognitive, and physiological dimensions of mental disorders, allowing for the assessment of symptom-like phenotypes and their underlying biological substrates [51–54].

Among preclinical approaches, genetically modified animal models have proven especially valuable, as they permit the targeted manipulation of specific genes implicated in disease-relevant pathways. By introducing gene deletions or structural alterations, transgenic models can approximate defined aspects of human pathology, thereby facilitating causal interpretations of gene-function relationships. Such models not only contribute to mechanistic understanding but also support translational research by enabling the evaluation of novel therapeutic strategies and the interpretation of clinical findings, including imaging and biomarker data [55–57].

Given the central role of the KYN pathway in shaping the neurochemical environment of the brain, enzymes regulating the formation of bioactive KYN metabolites represent particularly relevant targets for genetic manipulation [58–65]. Among these intermediates, KYNA occupies a prominent position due to its broad neuromodulatory profile. KYNA functions as an endogenous antagonist at the N-methyl-D-aspartate receptor and modulates excitatory neurotransmission through its interactions with α-amino-3-hydroxy-5-methyl-4-isoxazolepropionic acid and kainate receptors, while also influencing cholinergic signaling via the α7 nicotinic acetylcholine receptor. In addition, KYNA engages metabotropic signaling pathways through receptors such as G protein-coupled receptor 35 and the AhR, highlighting its capacity to influence neuronal and immune-related processes at multiple regulatory levels. Through these diverse interactions, KYNA plays a key role in maintaining excitatory-inhibitory balance and shaping synaptic and network-level activity [66, 67].

Alterations in KYNA availability have been associated with disrupted neurotransmission, cognitive deficits, and behavioral abnormalities, underscoring the importance of tightly regulated KYN pathway flux within the brain. Although substantial correlative evidence links KYNA dysregulation to neuropsychiatric conditions, experimental approaches that allow direct assessment of sustained KAT II deficiency *in vivo* have remained comparatively limited. This gap has constrained efforts to disentangle the primary effects of altered KYNA synthesis from secondary metabolic or adaptive changes within the KYN pathway [68].

To address this limitation, a novel *kat2*$^{-/-}$ mouse model was generated by our collaboration partners, Etsuro Ono and his colleagues (Kyushu University, Fukuoka, Japan), using CRISPR/Cas9-mediated gene editing on a C57BL/6N genetic background [69]. Female C57BL/6N mice were hormonally stimulated using pregnant mare serum gonadotropin,

followed by human chorionic gonadotropin administered at a 48-hour interval, after which they were mated with male C57BL/6N mice. Fertilized one-cell-stage embryos were subsequently collected from the oviducts and subjected to cytoplasmic microinjection with single guide RNA and recombinant Cas9 protein. The injected embryos were cultured to the two-cell stage and then transferred into pseudopregnant Institute for Cancer Research recipient females. The mouse strain generated through this procedure carries a targeted deletion within the *aadat* gene that results in the expression of a truncated KAT II polypeptide, effectively disrupting normal enzyme function. This CRISPR/Cas9 line carries an *aadat* deletion (KAT II knockout) and is referred to throughout as *kat2*$^{-/-}$. The strategy enabled precise genetic modification while preserving overall genomic integrity, providing a robust platform for studying the consequences of impaired KYNA synthesis under physiological conditions. The *kat2*$^{-/-}$ mouse model was designed to support an integrated analysis of behavioral phenotypes and their underlying metabolic correlates. Behavioral assessments focused on domains with established relevance to KYN pathway function, including emotional processing within the negative valence domain, learning and memory performance, and motor function. These domains were selected to capture behavioral features frequently altered in neuropsychiatric disorders and to evaluate the functional impact of disrupted KYNA regulation at the level of organisms.

In parallel, comprehensive profiling of Trp metabolism was performed to link behavioral outcomes to biochemical alterations. Levels of Trp and its metabolites were assessed across multiple metabolic pathways in peripheral samples, alongside measurements of enzyme activities related to Trp catabolism and indices of oxidative stress and excitotoxicity associated with KYN pathway metabolites. This multimodal approach enabled the identification of metabolic signatures associated with KAT II deficiency and provided a mechanistic context for the observed behavioral phenotypes.

By combining targeted genetic manipulation with behavioral and metabolic analyses, the *kat2*$^{-/-}$ mouse model constitutes a powerful experimental framework for investigating the role of KAT II and KYN pathway regulation in brain function. Importantly, this model allows for the differentiation between primary consequences of altered KYNA synthesis and secondary adaptations within interconnected metabolic networks, thereby offering valuable insight into the contribution of Trp metabolism to neuropsychiatric phenotypes.

Aims

I. Following the successful generation of the *kat2*$^{-/-}$ mouse model, our first objective was to verify the genetic background of the mouse colony before each experimental series. This step was essential to ensure that the gene knockout based on the *aadat* gene deletion was consistently present in all animals, thereby confirming the integrity of both the breeding strategy and the experimental cohorts.

II. Following confirmation of the appropriate genetic background, our next objective was to comprehensively assess the impact of reduced KAT II activity on the metabolic balance of Trp degradation pathways.

III. An additional aim of the study was the baseline phenotypic characterization of *kat2*$^{-/-}$ mice using standardized screening approaches to identify potential alterations in general health, neurological function, and sensorimotor performance that could influence subsequent behavioral assessments.

IV. Building on these metabolic and phenotypic findings, a further aim of the study was the behavioral characterization of *kat2*$^{-/-}$ mice, to determine how gene deletion-induced alterations in Trp metabolism may influence distinct behavioral domains.

Materials and methods

Animals

The C57BL/6N wild-type (WT) mice were obtained from Charles River Laboratories (Germany), while the *kat2*$^{-/-}$ mouse line was provided through collaboration with Kyushu University (Fukuoka, Japan) [69]. Animals were housed in polycarbonate cages (530 cm^2 floor area; 4-5 mice per cage) under specific pathogen-free conditions at the Animal Facility of the Department of Neurology, University of Szeged. Environmental parameters were maintained at 24 ± 1 °C, 45-55% relative humidity, and a 12-hour light-dark cycle. Mice had ad libitum access to standard laboratory chow and water, and environmental enrichment was provided using paper tubes, wooden blocks, and nesting material. The importation of genetically modified animals was authorized by the Department of Biodiversity and Gene Conversion of the Ministry of Agriculture (BGMF/37-5/2020). All experimental procedures complied with the Ethical Codex for Animal Experiments and were approved by the Ethics Committee of the Faculty of Medicine, University of Szeged, and the National Food Chain Safety Office (XI./84/2025 and X./1008/2025). The protocol for animal care was approved by the European Communities Council Directive (2010/63/EU) and the Hungarian Health Committee (40/2013 (II.14.)). Animal health was monitored weekly before the experiments and daily during the testing period using a standardized scoring system. Animals reaching predefined humane endpoints were excluded in accordance with welfare regulations.

I. Verification of the Genetic Background of the *kat2*$^{-/-}$ Mouse Model

All animals were genotyped before inclusion in any experimental procedure, ensuring verification of the genetic background before each experimental series. We collected tail biopsies under 2% isoflurane anesthesia, supplemented with topical lidocaine for local analgesia. A ~3 mm tail fragment was excised using sterile instruments under aseptic conditions, and tissue samples were stored at -80 °C until further processing. Genomic DNA was isolated using an alkaline lysis protocol adapted from the HotSHOT method [70]. Briefly, tissue samples were incubated in a freshly prepared lysis buffer containing 25 mM NaOH and 0.2 mM disodium EDTA at 95 °C for 30 minutes, followed by cooling and neutralization with 40 mM TRIS-HCl. This approach reliably yielded DNA suitable for downstream genotyping. DNA concentration and purity were assessed by spectrophotometry, and extracts were stored at -20 °C until analysis. Genotype determination was performed using a fluorescence-based

TaqMan allelic discrimination assay on a CFX Opus 96 real-time PCR system (Bio-Rad, USA). Reactions were run in singleplex format with allele-specific primers and dual-labeled probes. Each assay plate included non-template controls, as well as verified WT and *kat2*$^{-/-}$ reference samples. Allelic discrimination was based on endpoint fluorescence clustering, with genotype assignments cross-validated against amplification curves. Samples yielding ambiguous results were reanalyzed from the original DNA stock.

II. Metabolic Profiling of Tryptophan Degradation Pathways

Quantification of Tryptophan and Its Metabolites

8-week-old male *kat2*$^{-/-}$ and WT mice (n = 10 per group) were included in the metabolomic analyses. Urine samples were collected before anesthesia and immediately stored at -80 °C. For plasma collection, mice were anesthetized with 2% isoflurane, and blood samples were obtained from the left cardiac ventricle into tubes containing disodium ethylenediaminetetraacetate dihydrate. Plasma was separated by centrifugation (10,300 rpm, 10 minutes, 4 °C), transferred to fresh tubes, and stored at -80 °C until analysis. For central metabolite measurements, animals were perfused transcardially with artificial cerebrospinal fluid, after which brains were rapidly removed and dissected into the striatum (STR), cortex (CTX), hippocampus (HIPP), cerebellum (CER), and brainstem (STEM). All tissues were collected on ice and stored at -80 °C. Tissue sampling was performed between 08:00 and 12:00 to minimize circadian variability in Trp pathway measures.

Following tissue weight determination, brain samples were homogenized in three times their volume of ice-cold LC-MS-grade water using an ultrasonic homogenizer (UP100H, Hielscher Ultrasound Technology, Germany; 100% amplitude, 0.5 cycles). Samples failing predefined preparation or homogenization quality criteria were excluded before analysis. Targeted metabolomic profiling of Trp-KYN, serotonergic, indole-derived, and catecholaminergic metabolites, as well as selected cofactors, was performed using ultra-high-performance liquid chromatography coupled with tandem mass spectrometry (UHPLC-MS/MS), based on previously published and validated multiplex protocols [71, 72]. Analyses were conducted on a PerkinElmer Flexar UHPLC system coupled to an AB SCIEX QTRAP 5500 triple quadrupole mass spectrometer, operated with Analyst 1.7.1 software. Stable isotope-labeled internal standards were used to ensure accurate quantification. All reagents and solvents were of analytical or LC-MS grade.

Estimation of Enzymatic Activities

To estimate relative enzyme activities within the Trp metabolic network, product-to-substrate concentration ratios were calculated for each relevant enzymatic step [73–77]. This approach provides an indirect index of pathway flux and enzymatic engagement under the given experimental conditions. Ratio-based estimates were applied consistently across experimental groups, enabling comparative assessment of enzymatic balance within and between Trp degradation pathways.

Indices of Oxidative Stress and Excitotoxicity

An oxidative stress index (OSI) was derived by normalizing the concentration of the putative pro-oxidant 3-HK to the summed concentrations of the putative antioxidant metabolites KYNA, AA, and XA:

$$Oxidative\ stress\ index = \frac{[3-hydroxykynurenine]}{[Kynurenic\ acid] + [Anthranilic\ acid] + [Xanthurenic\ acid]}$$

An excitotoxicity index (EI) was calculated as the ratio of the NMDA receptor agonist QA to the NMDA receptor antagonist KYNA:

$$Excitotoxicity\ index = \frac{[Quinolinic\ acid]}{[Kynurenic\ acid]}$$

These indices were used to capture functional shifts in metabolic balance, rather than isolated changes in metabolites [78–82].

III. Baseline Phenotypic Characterization of *kat2*$^{-/-}$ Mice

8-week-old male *kat2*$^{-/-}$ and WT mice (n = 10 per group) underwent standardized baseline phenotypic assessment using the RIKEN-modified SHIRPA protocol, developed by The Institute of Physical and Chemical Research (RIKEN, Japan) [83–85]. All evaluations were performed between 08:00 and 12:00 to minimize circadian variability. Animals were transferred to the testing room one hour before scoring to allow for acclimatization. The SHIRPA protocol provides a comprehensive screen of general health, neurological status, and sensorimotor function and was applied to identify baseline phenotypic alterations that could confound subsequent behavioral testing. The assessment covered neuromuscular, autonomic, reflexive, and sensorimotor domains, including spontaneous activity, posture, locomotion, reflex integrity, and responses to sensory stimuli. All assessments were video-recorded using a Basler ace Classic acA1300-60gm camera (Basler AG, Germany) and analyzed with EthoVision XT14 software (Noldus Information Technology BV, The Netherlands).

IV. Behavioral Characterization of *kat2*$^{-/-}$ Mice

8-week-old male *kat2*$^{-/-}$ and WT mice (n = 10-13 per group) were included in the behavioral assessments. To ensure consistency across measurements, all behavior tests were conducted between 08:00 and 12:00. Before testing, animals were transferred to the experimental room one hour in advance to allow adequate acclimatization to the testing environment. Between individual animals, all behavioral apparatuses were cleaned with 70% ethanol and allowed to dry to minimize olfactory cues. For behavioral assays not requiring task-specific acquisition or analysis software, animal behavior was video-recorded and quantified using a Basler ace Classic acA1300-60gm camera (Basler AG, Ahrensburg, Germany) in combination with EthoVision XT14 software (Noldus Information Technology BV, Wageningen, The Netherlands), which served as the primary tools for behavioral tracking and data acquisition across multiple tests.

Open-field test (OFT)

The OFT was used to assess spontaneous locomotor and exploratory activity, as well as center-oriented exploration as an indirect index of anxiety-like behavior. Mice were tested individually in an open-field arena (48 × 40 cm) illuminated at the center by a standard table lamp. At the beginning of each session, animals were placed in the center of the arena and allowed to freely explore for 10 minutes [86, 87]. Locomotor and exploratory parameters were recorded using the Conducta 1.0 system (Experimetria Ltd., Budapest, Hungary), including ambulation, immobility, vertical and horizontal activity, jumping, rearing, and spatial distribution between central and corner zones.

Rotarod test

Motor coordination and balance were evaluated using an automated rotarod apparatus (TSE RotaRod V4.2.6, TSE Systems, Berlin, Germany). Mice underwent a two-day habituation and training period followed by testing on the third day. On Day 1, animals were placed individually on the rotating rod at 5 rpm for 3 minutes, with three trials performed at 30-minute intervals and immediate repositioning after falls. On Day 2, the procedure was repeated at a constant speed of 10 rpm. On Day 3, motor performance was assessed using an accelerating protocol (5-40 rpm over 3 minutes). Each mouse completed three test trials separated by 30-minute intervals without repositioning. Latency to fall was automatically recorded, and mean latency across trials was used for analysis [88–91].

Elevated Plus Maze (EPM) Test

Anxiety-like behavior was evaluated using the EPM, consisting of a plus-shaped apparatus elevated 50 cm above the floor, with two open and two enclosed arms (35 × 10 cm). Enclosed arms were bordered by 20 cm-high walls, while open arms lacked side walls. Mice were placed on the central platform facing an open arm and allowed to freely explore the maze for 5 minutes. Time spent in the open arms, closed arms, and central zone was recorded [92, 93].

Light Dark Box (LDB) Tests

Anxiety-like behavior was further assessed using the LDB test, comprising a larger illuminated compartment (two-thirds of the apparatus) and a smaller enclosed dark compartment (one-third), connected by a 5 × 5 cm opening. Mice were placed individually in the light compartment, and time spent in the illuminated area was recorded during a 5-minute session, beginning 5 seconds after placement to allow initial orientation [94–97].

Modified Forced Swim Test (FST)

Depressive-like behavior was evaluated using a modified FST. Mice were individually placed in a glass cylinder (12 cm diameter, 30 cm height) filled with fresh water (25 ± 1 °C) to a depth of 20 cm. To minimize novelty-related effects, a 15-minute pretest was conducted 24 hours before the 3-minute test session. During testing, immobility, swimming, and climbing behaviors were quantified using a time-sampling method [98, 99].

Tail Suspension Test (TST)

Depressive-like behavior was additionally evaluated using the TST. Animals were individually suspended by the tail for 6 minutes in a wooden enclosure (28.0 × 28.0 × 23.5 cm) using a clip attached to the top of the apparatus, allowing free limb movement without surface contact. Immobility duration was recorded as the primary outcome measure. To reduce discomfort and prevent tail injury, a cotton insert was placed inside the clip. Animals that climbed the clip or escaped suspension were excluded from analysis [100, 101].

Passive Avoidance Test (PAT)

PAT was used to assess fear-associated aversive learning and long-term memory. The apparatus consisted of two compartments with contrasting illumination, connected by a 5 × 5 cm opening. During the training session, mice were placed in the illuminated compartment and allowed to freely explore until entering the dark compartment, where a mild foot shock (0.3 mA) was delivered. Animals were removed from the apparatus 10 seconds later. Memory retention was evaluated 24 hours thereafter by recording the latency to enter the dark compartment. Mice that

did not enter the dark compartment within 5 minutes during training were excluded from further analysis [102–104].

Novel Object Recognition Test (NORT)

Recognition memory and novelty preference were assessed using NORT in a 60 × 60 × 60 cm arena. Three objects differing in shape and color, but matched for size, were used. The procedure was conducted over three consecutive days. On Day 1 (habituation), mice explored the empty arena for 10 minutes. During Day 2 (training), animals were allowed to explore two identical objects for 10 minutes; mice showing no object interaction were excluded from further analysis. On Day 3 (test), one familiar object was replaced with a novel object, while the remaining object served as the familiar control. Object-directed exploration time was recorded during training and testing [105–108]. Novelty preference was quantified using the discrimination index (DI) and preference index (PI), calculated as:

$$DI = \frac{Tnovel - Tfamiliar}{Tnovel + Tfamiliar}$$

$$PI = \frac{Tnovel}{Tnovel + Tfamiliar} \times 100$$

Object-Based Attention Test (OBAT)

Attentional performance was assessed using OBAT. The task was conducted in a two-compartment arena comprising a larger (40 × 40 × 40 cm) and a smaller (20 × 40 × 40 cm) compartment, using objects matched for size but differing in shape and color. During the training phase, mice explored five distinct objects in the larger compartment for 3 minutes. Animals failing to interact with the object later designated as familiar were excluded. In the test phase, the familiar object and a novel object were presented in the smaller compartment for 3 minutes. Object-directed exploration time during training and testing served as the primary outcome measure [109–111].

Y-Maze Test

Working memory performance was assessed using the Y-maze test. At the start of the trial, animals were placed at the distal end of the longest arm, facing the central junction, and allowed to freely explore the maze for 8 minutes. Spontaneous alternation behavior and the total number of arm entries were recorded [112–114]. The spontaneous alternation rate was calculated as follows:

$$Spontaneous\ alternation\ (\%) = \frac{number\ of\ spontaneous\ alternations}{total\ number\ of\ arm\ entries - 2} \times 100$$

Marble Burying Test (MBT)

Repetitive behavior was assessed using MBT. Mice were tested individually in a transparent plastic arena (40 × 24 × 18 cm) containing a 5 cm-deep layer of fresh bedding. Sixteen glass marbles (1 cm diameter) were arranged at one end of the arena in a regular grid pattern, with the outermost marbles positioned 3.5 cm from the walls and 5 cm spacing between adjacent marbles. The enclosure was covered with a ventilated transparent lid to prevent escape while allowing adequate airflow. Animals were allowed to freely explore the arena for 30 minutes, after which marbles were classified according to their degree of displacement or burial as intact, displaced, partially buried (0-75%), or fully buried (75-100%). The distribution of marble categories was quantified and compared across experimental groups [115–118].

Three Chamber Test (3CT)

Social behavior was evaluated using 3CT. For this type of behavioral test, we used a rectangular apparatus divided into three compartments (20.0 × 40.5 × 22.0 cm each) by opaque plastic walls with closable doorways (7.5 × 5.0 cm). Cylindrical wire-mesh enclosures placed in the lateral chambers permitted visual and olfactory interaction while preventing direct contact. The protocol comprised three phases. During habituation, mice were confined to the center chamber for 10 minutes. In the sociability phase, animals freely explored all compartments for 10 minutes, with one lateral chamber containing an empty enclosure and the other housing a novel, sex-, age-, and weight-matched conspecific. The social novelty phase followed an identical procedure, with the previously encountered animal serving as the familiar stimulus and a new conspecific introduced into the opposite chamber. Time spent in each compartment, enclosure investigation time, and chamber entries were recorded as primary outcome measures [119–123].

Statistical Analysis

All statistical analyses were performed using IBM SPSS Statistics, version 28.0.0.0 (IBM Corp., Armonk, NY, USA). Prior to inferential testing, the distribution of all datasets (metabolomic, phenotypic, and behavioral parameters) was assessed for normality using the Shapiro-Wilk test, complemented by visual inspection of Q-Q plots. Where appropriate, the Kolmogorov-Smirnov test was also applied. Homogeneity of variances was evaluated using Welch's F-test, and potential outliers were identified using Grubb's test. For comparisons

between *kat2*$^{-/-}$ and WT groups, independent samples t-tests were applied when assumptions of normality and variance homogeneity were met. In cases of non-normal distribution, the Mann-Whitney U test was used. Within-group comparisons of paired measures were analyzed using paired samples t-tests or Wilcoxon signed-rank tests, as appropriate. Data derived from paradigms involving multiple dependent variables or repeated factors were analyzed using mixed-design analysis of variance (ANOVA). When heterogeneity of variances was detected, Tamhane post hoc tests were applied. Baseline phenotypic data obtained using the SHIRPA protocol were analyzed using one-way ANOVA, reflecting their screening-level descriptive nature. Behavioral and metabolomic data were evaluated using two-tailed statistical tests throughout. A p-value < 0.05 was considered statistically significant for all analyses. Data are presented as mean ± standard deviation (SD).

Results

I. Verification of the Genetic Background of the *kat2*$^{-/-}$ Mouse Model

Genotyping procedures based on alkaline DNA extraction and TaqMan allelic discrimination were successfully established and consistently applied throughout the study. All *kat2*$^{-/-}$ animals included in the breeding program and experimental cohorts carried the targeted deletion, as confirmed before each experimental series (**Figure 2**). These results verify that the CRISPR/Cas9-mediated *aadat* deletion was stably maintained in a homozygous form across generations and did not exhibit loss or reversion during colony propagation.

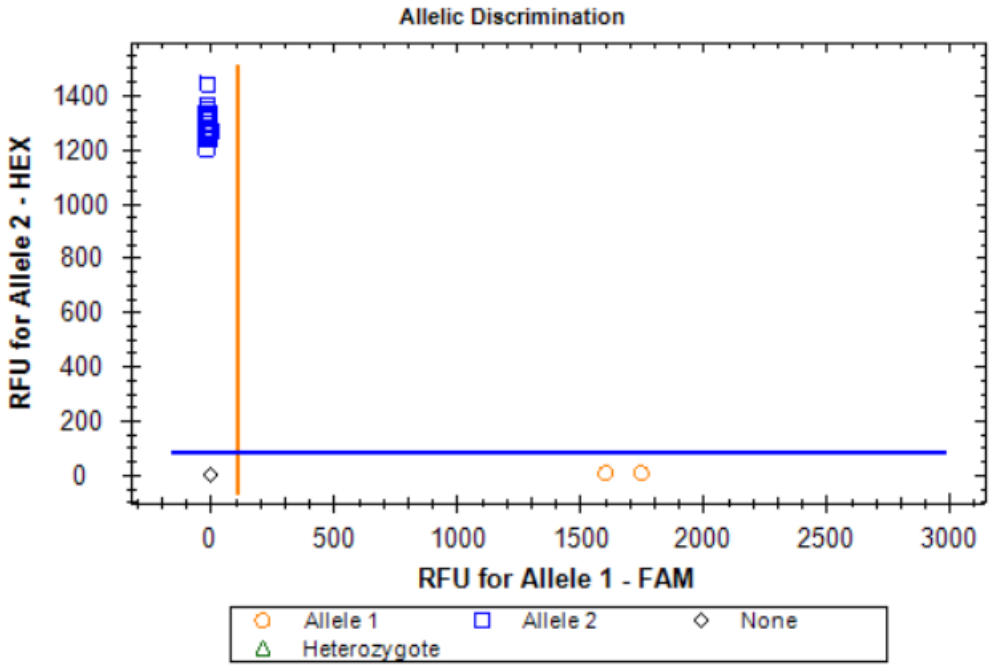

Figure 2. Representative TaqMan allelic discrimination plot used for genotypic verification of *kat2*$^{-/-}$ mice. Fluorescence intensity values are shown as relative fluorescence units for the WT-specific probe labeled with 6-carboxyfluorescein (FAM; Allele 1, x-axis) and the mutant allele-specific probe labeled with hexachloro-fluorescein (HEX; Allele 2, y-axis). Samples positive for Allele 1 (orange circles) correspond to WT mice, whereas samples positive for Allele 2 (blue squares) represent *kat2*$^{-/-}$ mice. Black diamonds indicate non-template controls lacking detectable amplification of either allele. Heterozygous samples, which would display concurrent FAM and HEX signals and be marked with green triangles, were not detected in the analyzed cohort, confirming homozygous inheritance of the deletion. Vertical and horizontal threshold lines indicate the fluorescence cutoffs used by the allelic discrimination algorithm to assign samples to allele-specific clusters. FAM, 6-carboxyfluorescein; HEX, hexachloro-fluorescein; RFU, relative fluorescence units.

II. Metabolic Profiling of Tryptophan Degradation Pathways

Quantification of Tryptophan and Its Metabolites

Targeted UHPLC-MS/MS analysis revealed widespread alterations in Trp-related metabolite profiles in *kat2*$^{-/-}$ mice compared to WT controls, affecting both peripheral matrices and distinct brain regions. In plasma, *kat2*$^{-/-}$ mice exhibited significantly reduced concentrations of KYN, KYNA, AA, XA, 5-HIAA, and IAA, accompanied by a marked elevation of 3-HK. In urine samples, the pattern was slightly different from that previously observed in plasma: KYNA,

XA, and IAA decreased, whereas KYN, 3-HK, and 5-HT increased relative to WT mice **(Figure 3, Figure 6**).

a) KYN

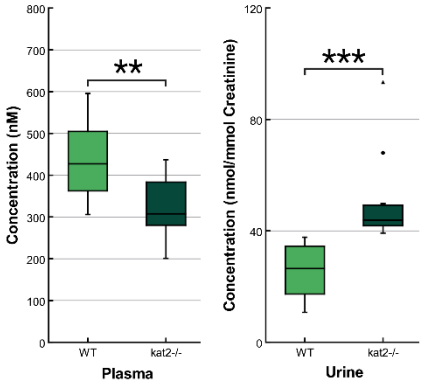

b) KYNA

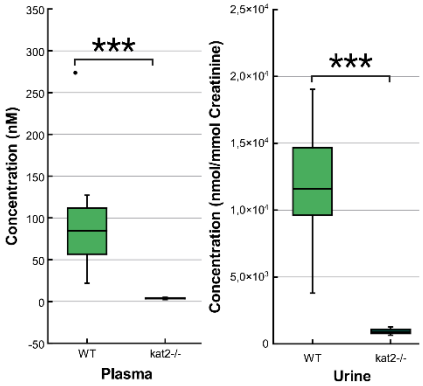

c) 3-HK

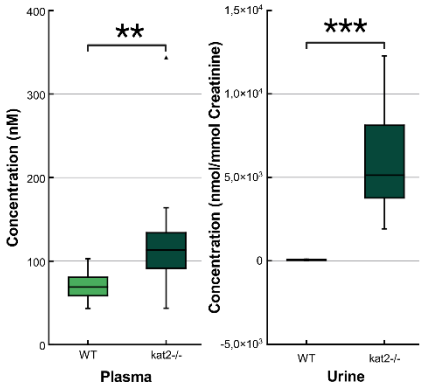

d) AA

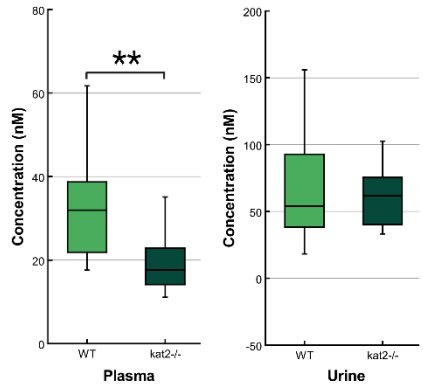

e) XA

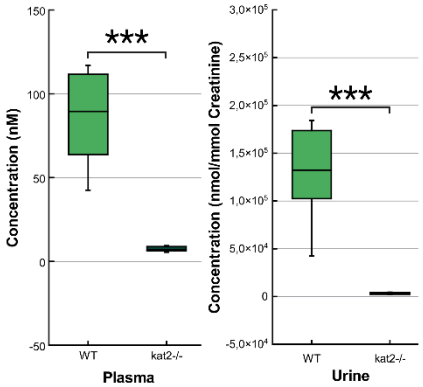

f) 5-HT

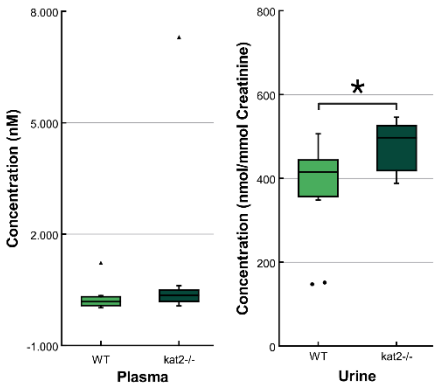

g) 5-HIAA

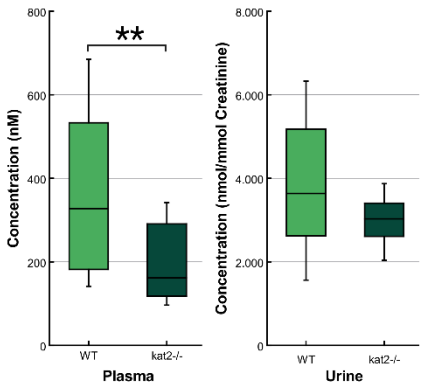

h) IAA

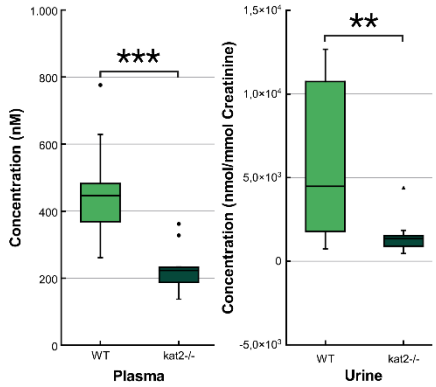

Figure 3. Peripheral concentrations of Trp-related metabolites in plasma and urine [69]. Results obtained from WT mice are indicated by light green boxes, whereas *kat2*$^{-/-}$ mice are represented by dark green boxes. Data are presented as mean ± SD. Statistical significance is denoted as * $p < 0.05$, ** $p < 0.01$, and *** $p < 0.001$. Outliers and extreme values are indicated by symbols. Figures were generated using LabPlot 2.9.0 (KDE, Berlin, Germany) and BioRender.com scientific illustration software. 3-HK, 3-hydroxykynurenine; 5-HIAA, 5-hydroxyindole-3-acetic acid; 5-HT, 5-hydroxytryptamine/serotonin; AA, anthranilic acid; IAA, indole-3-acetic acid; *kat2*$^{-/-}$, kynurenine aminotransferase II knockout mice; KYN, kynurenine; KYNA, kynurenic acid; XA, xanthurenic acid; WT, wild-type mice; •, outlier; ▲, far out.

Analysis of brain tissue demonstrated pronounced region-dependent metabolic remodeling (**Figure 4, Figure 6**). The most consistent alteration across all examined regions (STR, CTX, HIPP, CER, STEM) was an increase in 3-HK, accompanied by a global reduction in XA. In contrast, KYNA displayed a heterogeneous regional pattern, with significant decreases in CTX and HIPP, while being elevated in the STR. Despite these KYNA changes, its downstream metabolite QAA remained unchanged in CTX and HIPP but was significantly reduced in CER and STEM.

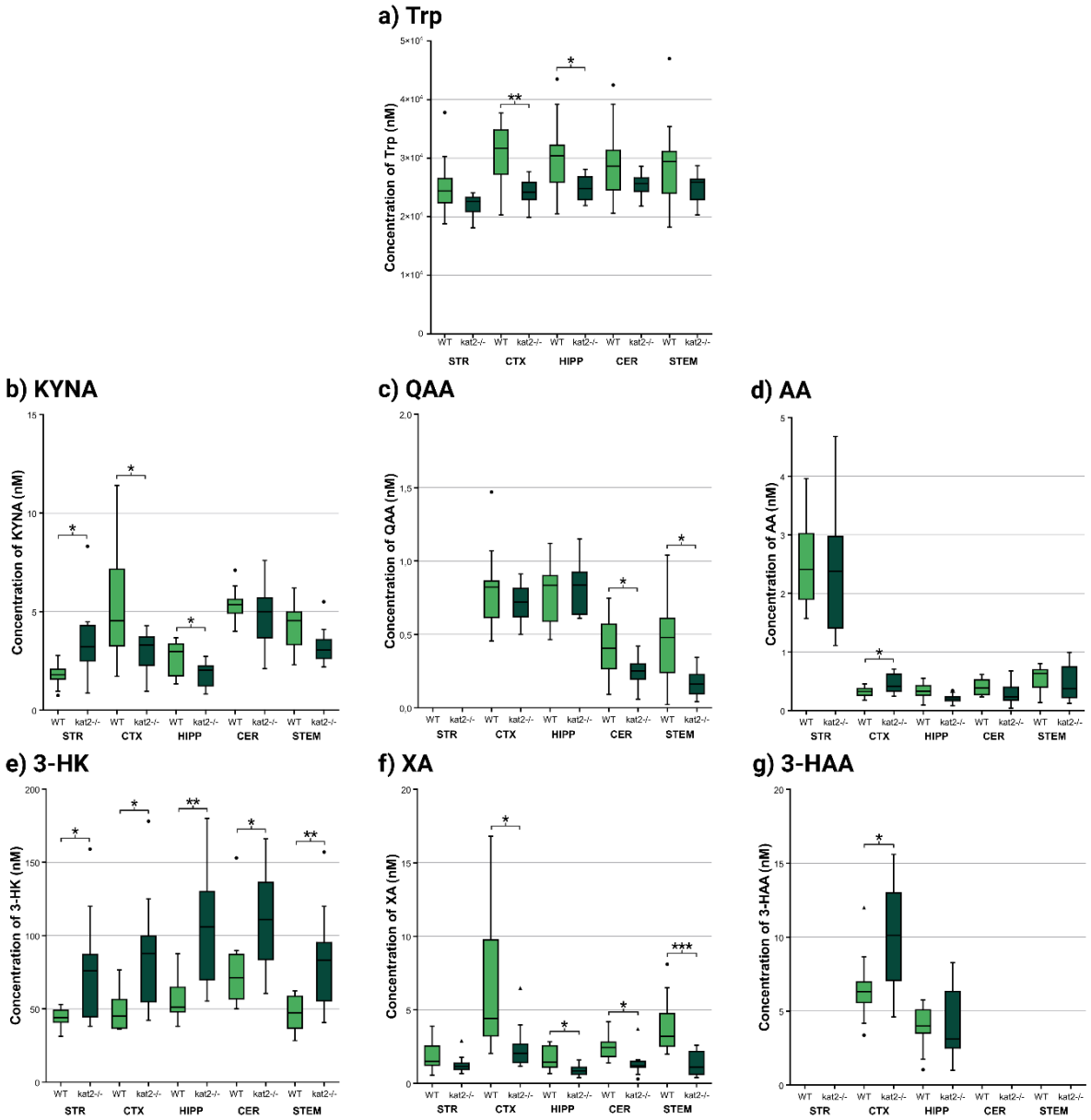

Figure 4. Brain region-dependent distribution of Trp and kynurenine pathway metabolites measured in *kat2*$^{-/-}$ and WT mice [11]. The figure displays quantitative data for Trp, KYNA, QAA, AA, 3-HK, XA, and 3-HAA. Results from WT mice are shown in light green, while *kat2*$^{-/-}$ mice are indicated in dark green. Data are presented as mean ± SD. Outliers and extreme values are marked accordingly. Statistical significance is denoted as * $p < 0.05$, ** $p < 0.01$, and *** $p < 0.001$. Figures were generated using LabPlot 2.9.0 (KDE, Berlin, Germany) and BioRender.com. 3-HAA, 3-hydroxyanthranilic acid; 3-HK, 3-hydroxykynurenine; AA, anthranilic acid; CER, cerebellum; CTX, cortex; HIPP, hippocampus; *kat2*$^{-/-}$, kynurenine aminotransferase II knockout mice; KYNA, kynurenic acid; QAA, quinaldic acid; STEM, brainstem; STR, striatum; Trp, tryptophan; WT, wild-type mice; XA, xanthurenic acid; •, outlier; ▲, far out.

Within the serotonergic pathway, 5-HTP levels were reduced in CTX and CER, whereas 5-HT concentrations were increased in CTX, consistent with the elevated urinary 5-HT observed peripherally (**Figure 5a-b, Figure 6**). Beyond the serotonergic system, selected metabolites of the indole-pyruvate pathway also exhibited region-specific alterations. IAA concentrations were reduced in the HIPP, while ICA levels were increased in the CTX. In the STEM, both ILA and INS concentrations were decreased relative to WT controls (**Figure 5c-f, Figure 6**). Additional alterations included reduced Tyr levels in CTX and HIPP, as well as selective decreases in pterin metabolites, together with alterations detected outside the core KYN pathway. To extend pathway coverage, metabolites of the indole-pyruvate and Tyr-DA pathways were also quantified. Among these, MHPGS emerged as the only metabolite showing a significant difference between genotypes, while other measured intermediates remained unchanged (**Figure 5g-j, Figure 6**).

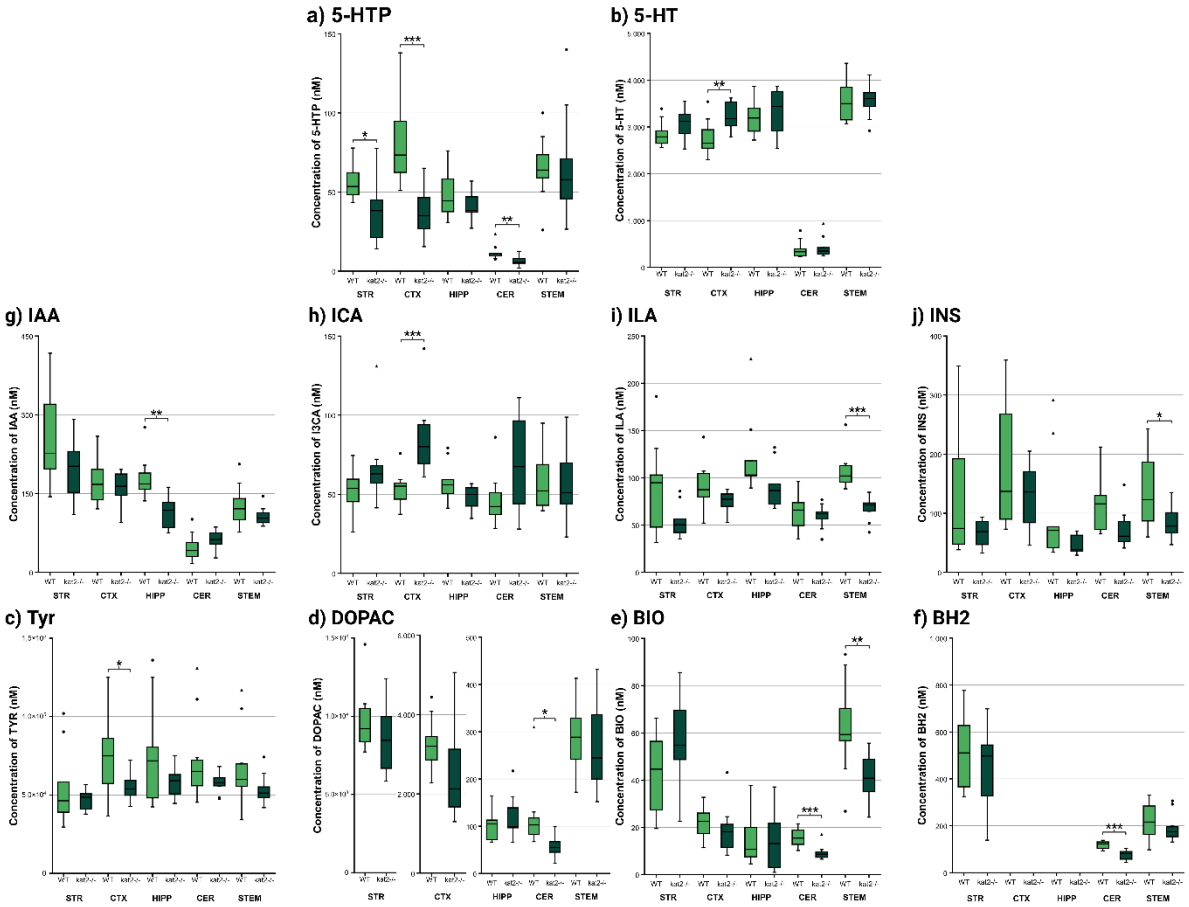

Figure 5. Regional concentrations of metabolites associated with the 5-HT, indole-pyruvate, and Tyr-DA pathways measured across distinct brain regions in *kat2*$^{-/-}$ and WT mice [11]. The figure presents box plots of serotonergic metabolites (a-b), indole-pyruvate pathway

metabolites (c-f), and Tyr-DA-related metabolites and cofactors (g-j) quantified in the STR, CTX, HIPP, CER, and STEM. Data from WT mice are shown in light green, whereas kat2-/- mice are indicated in dark green. Values are expressed as mean ± SD. The figure was generated with the use of LabPlot version 2.9.0 (KDE, Berlin, Germany) and BioRender.com. 5-HT, 5-hydroxytryptamine/serotonin; 5-HTP, 5-hydroxytryptophan; BH2, dihydrobiopterin; BIO, biopterin; CER, cerebellum; CTX, cortex; DOPAC, 3,4-dihydroxyphenylacetic acid; HIPP, hippocampus; IAA, indole-3-acetic acid; ICA, indole-3-carboxaldehyde; ILA, indole-3-lactic acid; INS, indoxyl sulfate; kat2-/-, kynurenine aminotransferase II knockout mice; STEM, brainstem; STR, striatum; Tyr, tyrosine; WT, wild-type mice; •, outlier; ▲, far out.

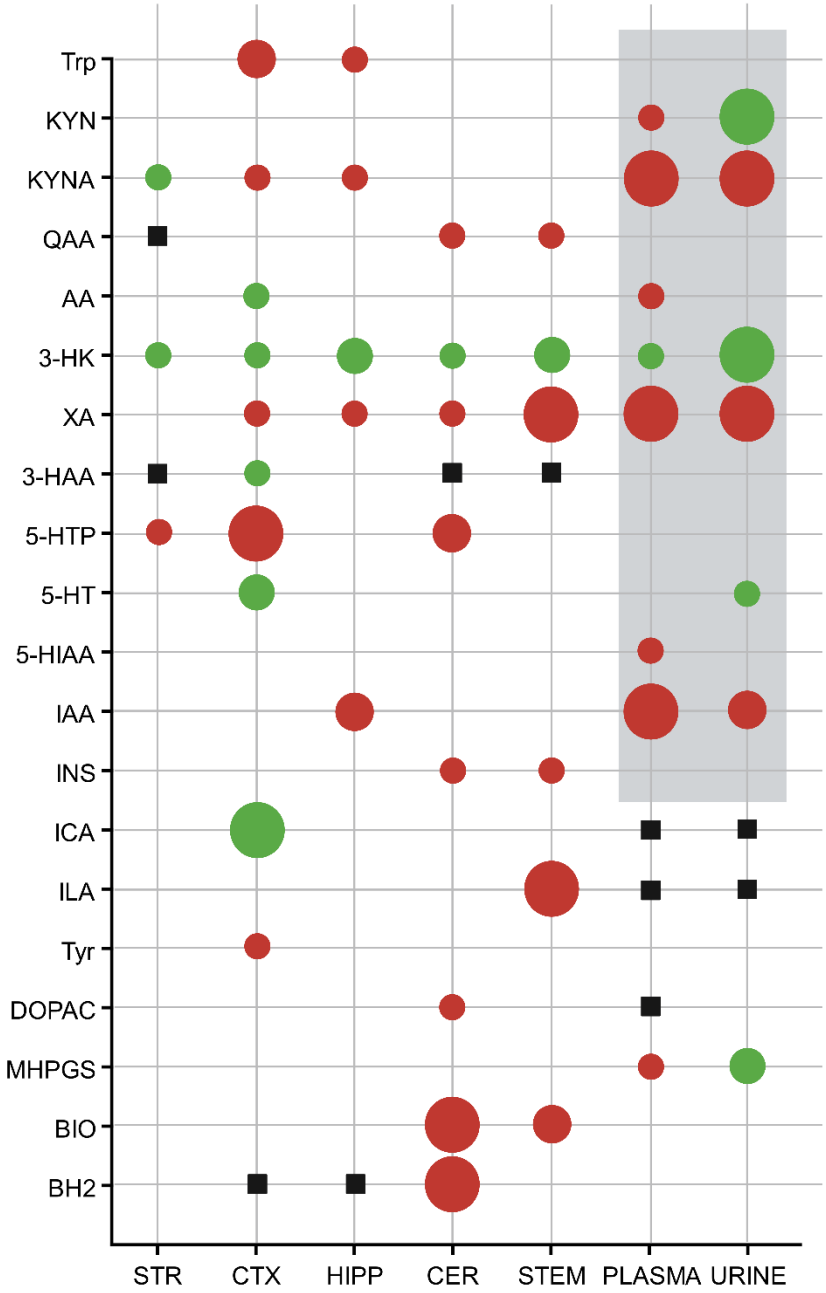

Figure 6. Summary of region- and matrix-specific differences in Trp-derived metabolites between *kat2*$^{-/-}$ and WT mice assessed by UHPLC-MS/MS [11]. Schematic overview of statistically significant changes in Trp-related metabolites across peripheral matrices (plasma, urine) and distinct brain regions (STR, CTX, HIPP, CER, STEM) in *kat2*$^{-/-}$ mice relative to WT controls. The diagram integrates alterations detected within the Trp-KYN, serotonergic, indole-pyruvate, and Tyr-DA pathways, providing a region- and matrix-resolved summary of the dataset. Statistically significant differences are indicated by colored circles, with red denoting decreased and green denoting increased metabolite concentrations compared to WT mice. The

size of the circles reflects the level of statistical significance (small: $p < 0.05$; medium: $p < 0.01$; large: $p < 0.001$). Gray background shading denotes data previously published in the first study, while the remaining data originate from the second manuscript. Black squares denote metabolites or matrices for which no data were available. The figure was created using LabPlot version 2.9.0 (KDE, Berlin, Germany) and BioRender.com. 3-HAA, 3-hydroxyanthranilic acid; 3-HK, 3-hydroxykynurenine; 5-HIAA, 5-hydroxyindole-3-acetic acid; 5-HT, 5-hydroxytryptamine/serotonin; 5-HTP, 5-hydroxytryptophan; AA, anthranilic acid; BH2, dihydrobiopterin; BIO, biopterin; CER, cerebellum; CTX, cortex; DOPAC, 3,4-dihydroxyphenylacetic acid; HIPP, hippocampus; IAA, indole-3-acetic acid; ICA, indole-3-carboxaldehyde; ILA, indole-3-lactic acid; INS, indoxyl sulfate; KYN, kynurenine; KYNA, kynurenic acid; MHPGS, 3-methoxy-4-hydroxyphenylglycol sulfate; QAA, quinaldic acid; STEM, brainstem; STR, striatum; Trp, tryptophan; Tyr, tyrosine; XA, xanthurenic acid.

Estimation of Enzymatic Activities

In plasma samples, *kat2*$^{-/-}$ mice exhibited significantly reduced estimated activities of KATs, KYNU, KAT III, monoamine oxidases (MAOs), aldehyde dehydrogenase (ALDH), and tryptophan-2-monooxygenase (TMO) relative to WT controls (**Figure 7**). In contrast, the estimated activity of KMO was significantly increased. In urine samples, a broadly similar pattern was observed, with lower estimated activities of KATs, KYNU, KAT III, MAO, ALDH, and TMO in *kat2*$^{-/-}$ mice compared to WT animals. In addition, higher estimated activities of TDO/IDOs, KMO, and aromatic L-amino acid decarboxylase (AADC) were detected in urine from *kat2*$^{-/-}$ mice.

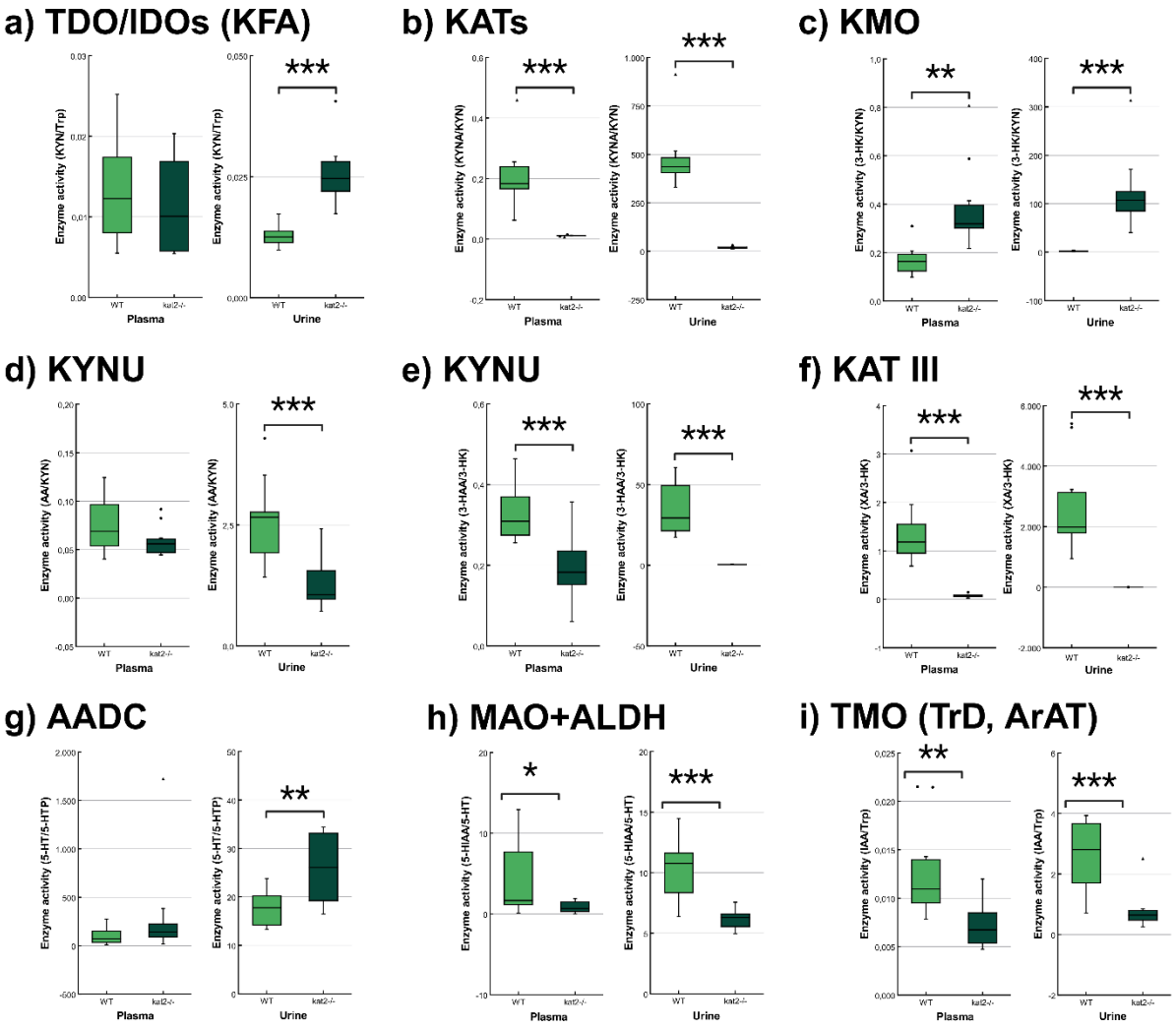

Figure 7. Estimated enzymatic activities within Trp metabolic pathways in plasma and urine [69]. The figure summarizes activity estimates for TDO/IDOs, KATs, KMO, KYNU, KAT III, AADC, MAO combined with ALDH, and TMO-related enzymatic steps. Data from WT mice are shown in light-colored boxes, whereas *kat2*$^{-/-}$ mice are indicated in dark-colored boxes. Results are expressed as mean ± SD. Levels of statistical significance are denoted by * $p < 0.05$, ** $p < 0.01$, and *** $p < 0.001$. Graphical representations were prepared using LabPlot version 2.9.0 (KDE, Berlin, Germany) and BioRender.com. 3-HAA, 3-hydroxyanthranilic acid; 3-HK, 3-hydroxykynurenine; 5-HIAA, 5-hydroxyindoleacetic acid; 5-HT, 5-hydroxytryptamine/serotonin; 5-HTP, 5-hydroxytryptophan; AA, anthranilic acid; AADC, aromatic L-amino acid decarboxylase; ALDH, aldehyde dehydrogenase; ArAT, aromatic amino acid aminotransferase; IAA, indole-3-acetic acid; IDOs, indoleamine 2,3-dioxygenases; KAT III, kynurenine aminotransferase III/cysteine conjugate beta-lyase 2; KATs, kynurenine aminotransferases; KFA, kynurenine formamidase; KMO, kynurenine 3-monooxygenase; KYN, kynurenine; KYNA, kynurenic acid; KYNU, kynureninase; MAO, monoamine oxidase;

TDO, tryptophan 2,3-dioxygenase; TMO, tryptophan-2-monooxygenase; TrD, tryptophan decarboxylase; Trp, tryptophan; XA, xanthurenic acid; •, outlier; ▲, far out.

Analysis of enzyme activity ratios demonstrated region-dependent alterations in estimated Trp metabolic fluxes in *kat2*$^{-/-}$ mice. KATs activity, expressed as the KYN/Trp ratio, was selectively reduced in the STR. In contrast, KMO activity was significantly increased across all examined regions. KYNU activity showed a modest but significant increase in the HIPP, whereas KAT III activity was consistently reduced in CTX, HIPP, CER, and STEM (**Figure 8a-d**). Within the serotonergic pathway, tryptophan hydroxylase (TPH) activity was reduced in CTX and CER, while AADC activity was increased in STR, CTX, and HIPP (**Figure 8e-g**). In addition, MAO/ALDH activity was decreased in the CTX. In the indole-pyruvate pathway, TMO activity was reduced in the CTX, HIPP, and CER (**Figure 8h**). Within the Tyr-DA pathway, MAO activity was reduced in the CER, while catechol-O-methyltransferase (COMT) activity was increased in the same region (**Figure 8i-j**).

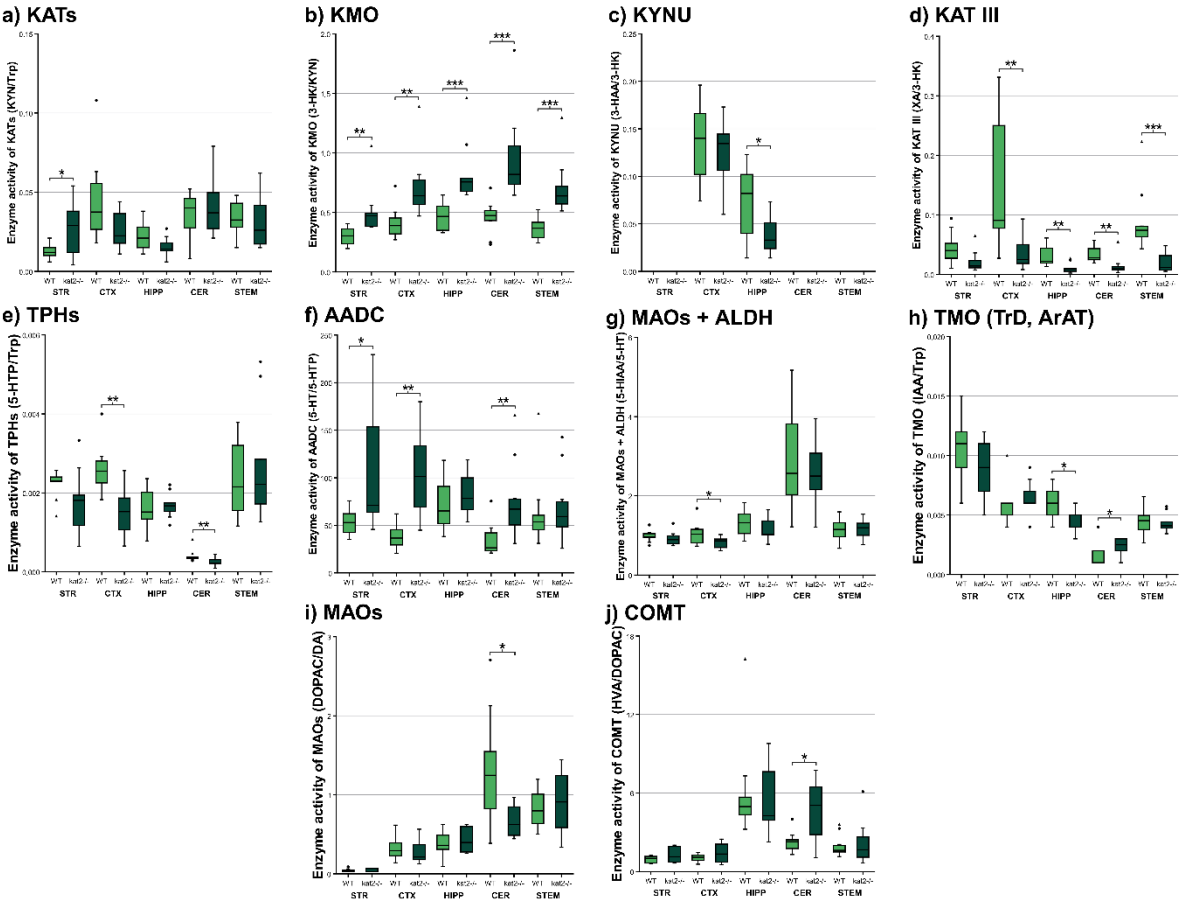

Figure 8. Region-specific alterations in estimated enzymatic activities across Trp-related metabolic pathways in *kat2*$^{-/-}$ and WT mice [11]. WT mice are represented by light-colored boxes, whereas *kat2*$^{-/-}$ mice are shown using dark-colored boxes. Box plots summarize activity

estimates in the STR, CTX, HIPP, CER, and STEM, calculated as product-to-substrate concentration ratios. Within the KYN pathway, enzymatic activities were estimated for KATs, KMO, KYNU, and KAT III (a-d). Within the serotonergic pathway, activity estimates included TPHs, AADC, and combined MAO/ALDH (e-g). Within the indole-pyruvate pathway, TMO-related activity was estimated using the IAA/Trp ratio (h). Within the Tyr-DA pathway, MAO and COMT activities were assessed (i-j). Data are presented as mean ± SD. Statistical significance is indicated as * $p < 0.05$, ** $p < 0.01$, and *** $p < 0.001$. Figures were generated using LabPlot 2.9.0 (KDE, Berlin, Germany) and BioRender.com. 3-HAA, 3-hydroxyanthranilic acid; 3-HK, 3-hydroxykynurenine; 5-HT, 5-hydroxytryptamine/serotonin; 5-HTP, 5-hydroxytryptophan; AADC, aromatic L-amino acid decarboxylase; ALDH, aldehyde dehydrogenase; ArAT, aromatic amino acid aminotransferase; CER, cerebellum; COMT, catechol-O-methyltransferase; CTX, cortex; DA, dopamine; DOPAC, 3,4-dihydroxyphenylacetic acid; HIPP, hippocampus; HVA, homovanillic acid; IAA, indole-3-acetic acid; KAT III, kynurenine aminotransferase III/cysteine conjugate beta-lyase 2; *kat2*$^{-/-}$, kynurenine aminotransferase II knockout mice; KATs, kynurenine aminotransferases; KMO, kynurenine-3-monooxygenase; KYN, kynurenine; KYNU, kynureninase; MAOs, monoamine oxidases; STEM, brainstem; STR, striatum; TMO, tryptophan-2-monooxygenase; TPHs, tryptophan hydroxylases; TrD, tryptophan decarboxylase; Trp, tryptophan; WT, wild-type mice; XA, xanthurenic acid; •, outlier; ▲, far out.

Indices of Oxidative Stress and Excitotoxicity

Indices of oxidative stress (**Figure 9a**) and excitotoxicity (**Figure 9b**) were significantly higher in both plasma and urine samples of *kat2*$^{-/-}$ mice compared to WT controls.

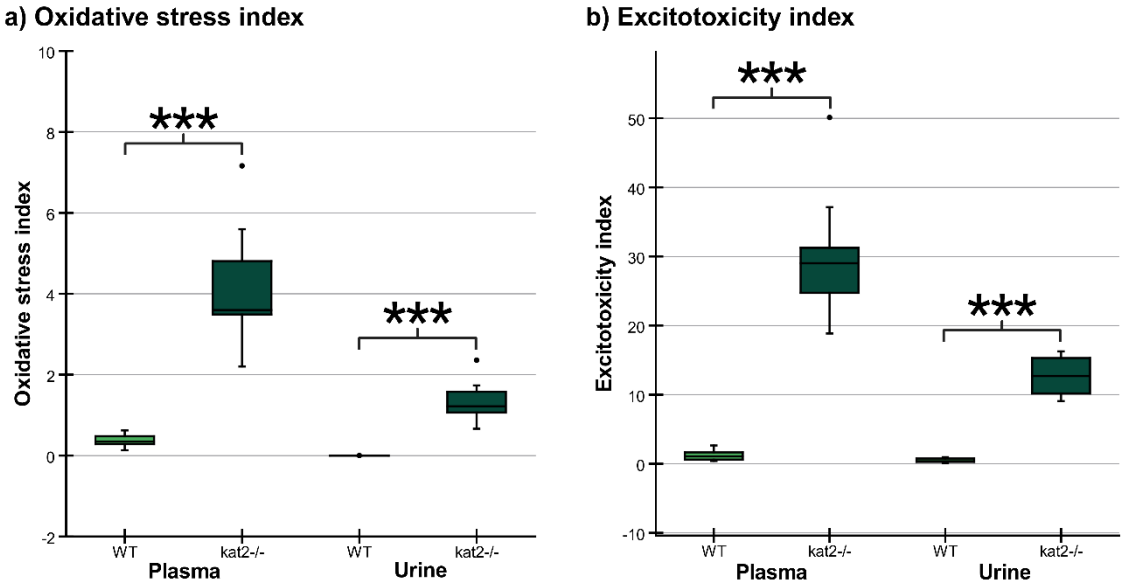

Figure 9. Peripheral OSI (a) and EI (b) measured in plasma and urine samples from *kat2*$^{-/-}$ and WT mice [69]. WT animals are represented by light-colored boxes, whereas *kat2*$^{-/-}$ mice are shown in dark-colored boxes. Data are presented as mean ± SD. Statistical significance is indicated as *** $p < 0.001$. The figure was generated with the use of LabPlot 2.9.0 (KDE, Berlin, Germany) and BioRender.com. *kat2*$^{-/-}$, kynurenine aminotransferase II knockout mice; WT, wild-type mice; •, outlier.

To assess oxidative stress and excitotoxicity within central compartments, composite indices were calculated from selected KYN pathway metabolites. The OSI (**Figure 10a**) was significantly elevated in several brain regions of *kat2*$^{-/-}$ mice, including the CTX, HIPP, CER, and STEM, with the largest increases observed in the HIPP and STEM. In contrast, the EI (**Figure 10b**) remained unchanged in the STR, CTX, and CER, whereas a significant increase was observed in the HIPP.

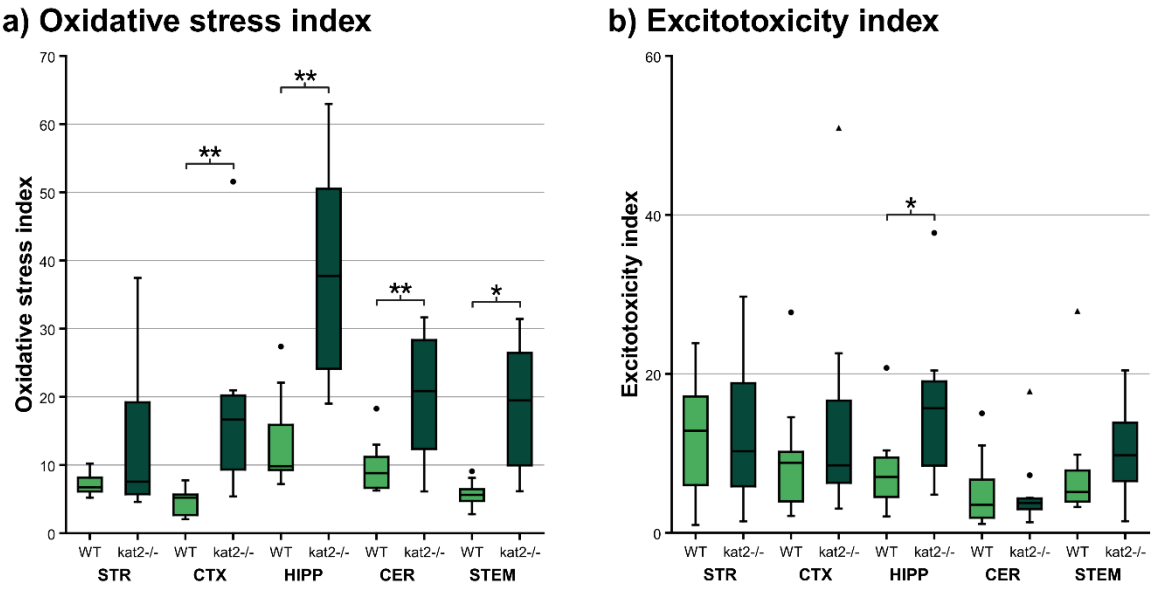

Figure 10. Region-specific (a) OSI and (b) EI in *kat2*$^{-/-}$ and WT mice [11]. Box plots depict index values in the STR, CTX, HIPP, CER, and STEM. WT animals are shown in light-colored boxes, whereas *kat2*$^{-/-}$ mice are represented by dark-colored boxes. Data are presented as mean ± SD. Statistical significance is indicated as * $p < 0.05$, and ** $p < 0.01$. The figure was prepared using LabPlot 2.9.0 (KDE, Berlin, Germany) in combination with BioRender.com. CER, cerebellum; CTX, cortex; HIPP, hippocampus; *kat2*$^{-/-}$, kynurenine aminotransferase II knockout mice; STEM, brainstem; STR, striatum; WT, wild-type mice; •, outlier; ▲, far out.

III. Baseline Phenotypic Characterization of *kat2*$^{-/-}$ Mice

Baseline phenotypic assessment using the modified SHIRPA test revealed no significant differences between *kat2*$^{-/-}$ mice and their WT counterparts across the evaluated parameters.

IV. Behavioral Characterization of *kat2*$^{-/-}$ Mice

Locomotor Activity and Motor Coordination

Baseline locomotor activity and motor coordination were assessed using OFT and rotarod paradigms. In OFT, *kat2*$^{-/-}$ mice exhibited a reduction in spontaneous locomotor activity, as reflected by a significantly shorter ambulation distance during the 10-minute observation period compared to WT controls (**Figure 11a**). In addition, *kat2*$^{-/-}$ mice performed fewer jumps (**Figure 11b**) and showed reduced exploratory behavior, indicated by a lower number of entries into both the center and corner zones of the arena (**Figure 11c**). Although OFT captures multiple behavioral components, anxiety-related parameters were further examined using dedicated tests described below.

In contrast, performance on the rotarod task did not differ between genotypes, and no significant strain-dependent differences were detected in parameters reflecting motor coordination or motor learning. Together, these findings indicate subtle alterations in spontaneous locomotor and exploratory activity in the genetically modified mice, while motor coordination and balance remained preserved.

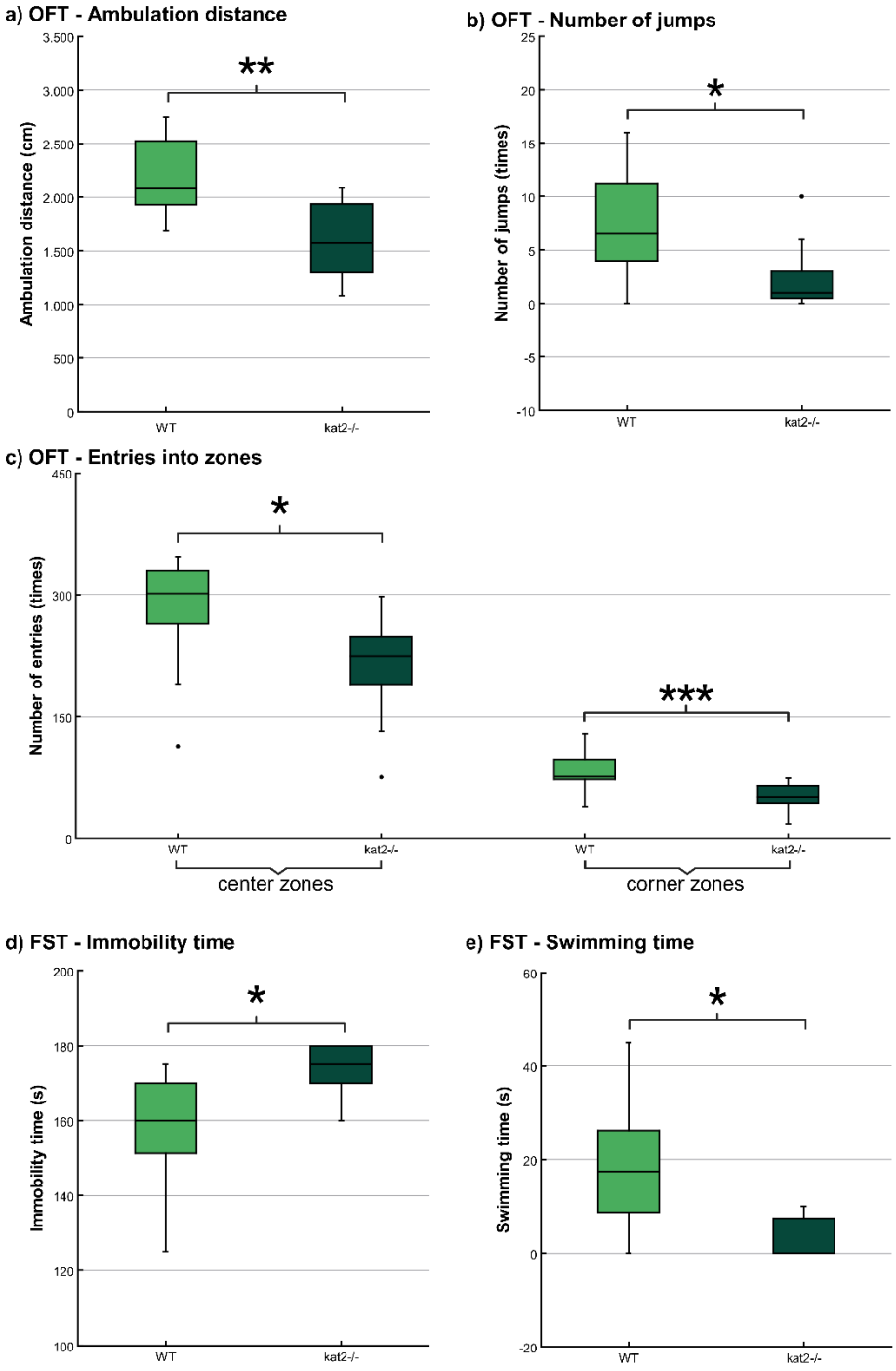

Figure 11. Behavioral parameters exhibiting significant inter-strain differences between *kat2*$^{-/-}$ and WT mice [69]. Box plots depict OFT parameters showing statistically significant genotype-dependent differences: (a) ambulation distance, (b) number of jumps, and (c) entries into the center and corner zones. Modified FST measures showing significant inter-strain differences are (d) time spent immobile and (e) time spent swimming. WT mice are represented by light green boxes, whereas *kat2*$^{-/-}$ mice are shown in dark green. Data are presented as mean ± SD.

Statistical significance is indicated as * $p < 0.05$, ** $p < 0.01$, and *** $p < 0.001$. The figure was prepared using LabPlot 2.9.0 (KDE, Berlin, Germany) in combination with BioRender.com. FST, forced swim test; *kat2*$^{-/-}$, kynurenine aminotransferase II knockout mice; OFT, open-field test; WT, wild-type mice; •, outlier.

Anxiety-Like Behavior

Anxiety-related behaviors were evaluated using EPM, LDB and MBT paradigms. Across all measured parameters, no significant genotype-dependent differences were detected between *kat2*$^{-/-}$ mice and WT controls, indicating comparable anxiety-like behavior under the applied testing conditions.

Depression- and Stress-Related Behavior

Depression- and stress-related behaviors were examined using the modified FST and TST. In FST, *kat2*$^{-/-}$ mice displayed a significantly longer immobility time (**Figure 11d**) accompanied by a reduced swimming time (**Figure 11e**) compared to WT controls. In contrast, no statistically significant genotype-dependent differences were observed in TST.

Cognitive and Attentional Performance

Cognitive and attentional functions were evaluated using tasks assessing recognition memory, attentional allocation, working memory, and aversive learning. In NORT, both *kat2*$^{-/-}$ and WT mice spent significantly more time exploring the novel object compared to the familiar one during the test phase, with no significant differences detected between genotypes in exploration time or discrimination indices. Performance in PAT did not differ between the genetically modified and WT mice, as measured by step-through latency during the retention trial. In OBAT, total object exploration time during both the training and testing phases was comparable between strains. Within the *kat2*$^{-/-}$ group, animals spent significantly more time interacting with the novel object than with the familiar one during the testing phase, whereas no between-strain differences were observed. Assessment of spatial working memory in the Y-maze test revealed no significant genotype-dependent differences in spontaneous alternation rates or total arm entries.

Repetitive and Social Behavior

In 3CT, both *kat2*$^{-/-}$ and WT mice spent significantly less time in the lateral compartments than in the central chamber during both the sociability and social novelty phases. Beyond this shared spatial preference, no genotype-dependent differences were detected across any of the measured social interaction parameters.

Discussion

Genetic validation and model integrity

Interpreting metabolic and behavioral outcomes requires a genetically stable, well-validated experimental model. In this study, systematic genotyping confirmed that the *aadat* deletion was consistently present in all animals assigned to the knockout group across experimental cohorts. The absence of heterozygous genotypes, together with clear segregation between *kat2*$^{-/-}$ and WT alleles, indicates stable homozygous inheritance of the CRISPR/Cas9-mediated deletion without evidence of allelic reversion or mosaicism. The robustness of the genotyping workflow, combining alkaline DNA extraction with fluorescence-based TaqMan allelic discrimination, ensured high specificity and reproducibility of genotype assignment. This methodological consistency minimized the risk of genetic misclassification and excluded inadvertent inclusion of animals with partial or ambiguous genotypes. As a result, phenotypic variability attributable to background genetic drift or incomplete gene disruption can be reasonably excluded. Importantly, the confirmed integrity of the *kat2*$^{-/-}$ line strengthens causal attribution between KAT II deficiency and the observed metabolic remodeling. It further supports the interpretation that downstream biochemical and functional alterations reflect genuine consequences of KAT II loss rather than secondary effects of breeding instability. This validated genetic foundation provides a necessary framework for assessing how targeted disruption of a single enzymatic node propagates across interconnected Trp metabolic pathways.

Metabolic remodeling and pathway dominance following KAT II deletion

Genetic deletion of KAT II induced a coordinated yet spatially heterogeneous reorganization of Trp metabolism across peripheral and central compartments. In plasma and urine, the metabolic profile consistently shifted toward elevated 3-HK, accompanied by reduced KYNA and XA levels, indicating redistribution of KYN pathway flux away from antioxidant and toward pro-oxidant branches. These peripheral changes were paralleled by alterations in serotonergic and indole-derived metabolites, underscoring that KAT II loss perturbs multiple interconnected Trp-derived pathways rather than selectively affecting KYNA synthesis.

Within the brain, metabolic remodeling exhibited pronounced regional specificity. A uniform elevation of 3-HK across all examined regions contrasted with a global reduction of XA, reflecting a widespread pro-oxidant biochemical bias. In contrast, KYNA levels diverged regionally, decreasing in cortical and hippocampal regions while increasing in the STR,

suggesting the engagement of local compensatory mechanisms that differentially shape KYN metabolism. These patterns indicate that central Trp metabolism is governed primarily by regional enzymatic context rather than by peripheral metabolite availability alone. Partial concordance between central and peripheral signatures, particularly for elevated 3-HK and reduced XA, nevertheless supports shared overarching trends across compartments.

Product-to-substrate ratios further revealed a marked reweighting of enzymatic fluxes following KAT II deletion. Across matrices, inferred KMO activity was consistently elevated, aligning with robust 3-HK accumulation and indicating a dominant shift toward the oxidative branch of the pathway. In parallel, reduced KAT-associated fluxes, including those linked to XA formation, were evident in multiple brain regions, further constraining protective routes. Importantly, these changes were region-dependent rather than uniform, delineating pathway dominance shaped by local metabolic demands. Collectively, these findings define a metabolic hierarchy in which KMO-driven flux predominates while KAT-mediated buffering is constrained, creating a functional basis for downstream biochemical vulnerability.

Importantly, targeted manipulation of a single KYN-pathway enzyme propagates across the broader Trp metabolic network rather than remaining confined to the pathway. Deletion of KAT II, while directly impairing KYNA synthesis, concurrently perturbed the balance of 5-HT, indole-pyruvate, and interconnected Tyr-DA pathways. The parallel alterations observed across these systems suggest that Trp metabolism operates as an integrated network, in which enforced redirection of flux within one branch propagates secondary adjustments in competing pathways through shared substrates, cofactors, and redox-sensitive regulatory nodes. Thus, KAT II deficiency should be viewed not as a pathway-restricted perturbation, but as a systems-level disturbance reshaping monoaminergic and indole-derived metabolic equilibrium.

Latent oxidative and excitotoxic vulnerability

Deletion of KAT II establishes a metabolic environment characterized by elevated oxidative pressure and context-dependent excitotoxic susceptibility across both central and peripheral compartments. Composite indices derived from KYN metabolites revealed a consistent pro-oxidant shift in *kat2*$^{-/-}$ mice. OSI increased in multiple brain regions (CTX, HIPP, CER, STEM) and in peripheral samples (plasma, urine), indicating a systemic redox shift following impaired KYNA synthesis rather than a purely central effect. This pattern was primarily driven by robust elevation of 3-HK combined with reduced antioxidant buffering capacity.

Similarly, EI was elevated in peripheral matrices, reflecting a global shift toward reduced excitatory antagonism relative to neurotoxic drive. In contrast, within the brain, excitotoxic vulnerability displayed pronounced regional specificity. A significant increase in EI was confirmed in HIPP, suggesting that excitatory-inhibitory balance is differentially regulated across neural circuits. This dissociation indicates that while peripheral indices capture a generalized vulnerability state, central excitotoxic risk is gated by region-specific buffering mechanisms and metabolic context.

Importantly, the convergence of increased OSI and EI does not translate into overt neurotoxicity or baseline behavioral impairment. Instead, KAT II deficiency defines a latent vulnerability state, in which oxidative stress and reduced glutamatergic antagonism lower the threshold for dysfunction without precipitating immediate pathology. Peripheral elevations in vulnerability indices further support the presence of a whole-body metabolic predisposition that parallels but does not dictate regional brain susceptibility.

These findings support the interpretation that oxidative stress and excitotoxicity function as permissive conditions shaping circuit resilience, thereby priming stress-sensitive regions, particularly the hippocampus, for dysfunction in response to secondary challenges such as stress, aging, or inflammatory load.

Behavioral resilience despite neurochemical imbalance

Despite the pronounced and regionally heterogeneous metabolic alterations across Trp-derived pathways, *kat2*$^{-/-}$ mice displayed largely preserved baseline phenotype and behavioral integrity. Comprehensive screening using the modified SHIRPA protocol revealed no genotype-dependent differences in general appearance, autonomic signs, sensorimotor reflexes, or basic neurological function, indicating that deletion of KAT II does not impair fundamental physiological or developmental processes in young adulthood. This phenotypic stability is notable given the marked neurochemical imbalance characterized by altered enzymatic fluxes, elevated OSI, and region-specific shifts in KYN intermediates, and underscores the capacity of compensatory mechanisms to buffer substantial metabolic perturbations under baseline conditions.

Behavioral assessment further supported a dissociation between neurochemical state and functional output. Alterations were restricted to tasks probing spontaneous exploration and stress coping, whereas anxiety-like behavior, cognitive performance, social interaction, and aversive memory remained largely intact. In the OFT, the genetically modified mouse strain

exhibited reduced exploratory engagement, reflected by decreased ambulation and zone transitions, without evidence of motor impairment or heightened anxiety. In parallel, the modified FST revealed increased immobility accompanied by reduced active coping, consistent with altered stress responsivity. Importantly, this pattern was not mirrored in the TST, highlighting that these paradigms capture distinct dimensions of stress-related behavior rather than a unitary depressive construct.

From a translational perspective, this behavioral dissociation bears relevance to neuropsychiatric conditions in which profound biochemical or metabolic abnormalities coexist with subtle or context-dependent behavioral manifestations. In disorders such as major depression or trauma-related syndromes, metabolic vulnerability and altered stress processing may precede or outpace overt symptom expression, emerging clinically only under sustained stress or environmental challenge. Viewed translationally, the *kat2*$^{-/-}$ mice model stress-sensitive affective bias rather than a full disease state: neurochemical imbalance shifts coping strategies without generating broad baseline behavioral pathology. Such a framework supports the utility of this model for investigating mechanisms of susceptibility and resilience relevant to neuropsychiatric vulnerability.

Limitations and future directions

Several limitations should be considered when interpreting the present findings. First, the study was conducted under baseline conditions in young adult male mice, which restricts conclusions regarding developmental trajectories, aging-related effects, or sex-dependent differences. Given the well-documented sexual dimorphism in Trp metabolism and stress responsivity, inclusion of female cohorts and longitudinal designs will be essential to determine whether KAT II-related vulnerabilities emerge or diverge across lifespan stages.

Second, metabolomics relies on bulk tissue homogenates, which collapse cell-type-specific signals by averaging metabolites across heterogeneous cellular populations. Astrocytes, neurons, microglia, and endothelial cells contribute differentially to KYN, serotonergic, and indole-pyruvate pathway fluxes, and cell-type-specific alterations may be masked in regional homogenates. Future studies incorporating cell-resolved approaches – such as single-cell or spatial metabolomics, or cell-type-specific genetic manipulations – will be necessary to localize metabolic rewiring within defined circuit elements.

Third, enzymatic activities were inferred from product-to-substrate ratios rather than directly measured enzyme kinetics. While this strategy provides robust functional proxies at the systems

level, it cannot fully resolve regulatory mechanisms such as post-translational modification, compartmentalization, or cofactor availability. Complementary approaches, including isotope tracing or targeted enzyme assays, would refine causal interpretation of pathway dominance.

Fourth, the gut microbiota was not directly characterized. Although indole-derived metabolites were quantified centrally and peripherally, the absence of taxonomic or functional microbiome data limits inference regarding microbial contributions to the observed metabolic shifts. Integrating fecal metagenomics, metatranscriptomics, and microbial metabolite profiling will be critical for dissecting host-microbiota interactions within this framework.

Finally, behavioral testing did not incorporate stress challenges or cognitive load manipulators. Given the evidence for latent metabolic vulnerability, future work should employ paradigms that tax emotional regulation, attentional flexibility, or stress coping to unmask context-dependent phenotypes. Such designs will be pivotal for translating biochemical risk signatures into functionally meaningful outcome measures.

Conclusions

This study provides an integrated characterization of the neurochemical and behavioral consequences of genetic deletion of the *aadat* gene, which encodes KAT II, by combining region-resolved metabolomics, inferred enzymatic fluxes, OSI and EI, and a multidomain behavioral phenotyping battery in young adult *kat2*$^{-/-}$ mice. Loss of KAT II resulted in pronounced and spatially heterogeneous remodeling of Trp metabolism across central and peripheral compartments, while behavioral alterations remained selective, modest, and context dependent.

At the biochemical level, *aadat* deletion shifted Trp degradation toward a pro-oxidant and potentially excitotoxic profile, characterized by pan-regional elevation of 3-HK, reduced XA, region-specific modulation of KYNA, and altered flux through serotonergic, indole-pyruvate, and catecholaminergic pathways. These changes were accompanied by increased OSI and EI, particularly within cortico-hippocampal regions, indicating latent metabolic vulnerability rather than overt neurodegeneration. Concordant alterations in plasma and urine support the translational relevance of peripheral readouts as indicators of central pathway imbalance.

Despite this marked neurochemical disequilibrium, baseline behavioral performance across most cognitive, social, and anxiety-related domains was largely preserved, highlighting the capacity of neural systems to buffer substantial metabolic perturbations under non-challenging conditions. Nonetheless, selective behavioral differences emerged in paradigms probing spontaneous exploration and stress coping. Reduced exploratory activity in OFT and increased immobility in the modified FST indicate altered engagement and stress responsivity, without corresponding effects in TST or aversive memory tasks.

Overall, these findings support a model in which KAT II deficiency establishes a state of metabolic and affective susceptibility rather than constitutive psychopathology. By refining the role of KAT II within the KYN pathway and complementary branches of Trp metabolism, this work provides a mechanistic framework for future studies exploring how metabolic dysregulation contributes to neuropsychiatric vulnerability and may inform the development of pathway-targeted therapeutic strategies.

Acknowledgement

I would like to express my sincere gratitude to my supervisors, Professor László Vécsei and Dr. Masaru Tanaka, for their continuous guidance, professional advice, and support throughout my doctoral studies. I am especially thankful for their role in shaping my scientific thinking and for their assistance in my academic and scientometric development.

I also thank Professor Péter Klivényi, Head of Department, for providing the opportunity to conduct my doctoral work and related research at the Department of Neurology.

I am grateful to all current and former members of the HUN-REN–SZTE Neuroscience Research Group, with special thanks to Dr. Diána Martos, Dr. Zsuzsanna Fülöpné Bohár, Dr. Annamária Fejes-Szabó, and Dr. Eleonóra Spekker, whose support and mentorship greatly contributed to my scientific progress. I would also like to thank our laboratory assistant, Erzsébet Lukács, for her invaluable help with the technical aspects of laboratory work.

I extend my appreciation to our collaboration partners, Dr. Zsolt Galla, Dr. Péter Monostori, Dr. László Juhász, Krisztina Spisák, Dr. Mónika Szűcs, Professor Mihály Boros, and Professor József Toldi, whose professional input and fruitful cooperation significantly advanced our research. Additionally, I am deeply thankful to Professor Etsuro Ono and his colleagues at Kyushu University, Fukuoka, for providing the genetically modified mouse strains essential for this work.

Finally, I would like to express my deepest gratitude to my beloved family and friends for their unconditional love, patience, continuous support, and for standing by me and believing in me throughout these challenging years. *"**Sub pondere crescit palma.**"*

This work was financially supported by the GINOP-2.3.2-15-2016-00034 grant, the National Research, Development, and Innovation Office–NKFIH (K138125), the SZTE SZAOK-KKA program (No. 2022/5S729), the HUN-REN Hungarian Research Network, the Japan Society for the Promotion of Science (JSPS) through its Joint Research Projects under Bilateral Programs (Grant No. JPJSBP120203803), and the Hungarian Academy of Sciences (NKM-65/1/2021). During my doctoral studies, I received partial support from the Doctoral School of Clinical Medicine, Albert Szent-Györgyi Medical School, University of Szeged.

During the preparation of my thesis, I used Grammarly and ChatGPT 5.2 for grammar checking, correction, and refinement of scientific language.

References

[1] D. Li *et al.*, "Tryptophan metabolism: Mechanism-oriented therapy for neurological and psychiatric disorders," *Front. Immunol.*, vol. 13, Sep. 2022, doi: 10.3389/FIMMU.2022.985378.

[2] E. L. Gibson, "Tryptophan supplementation and serotonin function: genetic variations in behavioural effects," *Proc. Nutr. Soc.*, vol. 77, no. 2, pp. 174–188, May 2018, doi: 10.1017/S0029665117004451.

[3] Y. Huang *et al.*, "Tryptophan Metabolism in Central Nervous System Diseases: Pathophysiology and Potential Therapeutic Strategies," *Aging Dis.*, vol. 14, no. 3, pp. 858–878, Jun. 2023, doi: 10.14336/AD.2022.0916.

[4] M. Tanaka, Z. Bohár, and L. Vécsei, "Are kynurenines accomplices or principal villains in dementia? Maintenance of kynurenine metabolism," *Molecules*, vol. 25, no. 3. MDPI AG, Jan. 28, 2020, doi: 10.3390/molecules25030564.

[5] J. Savitz, "The kynurenine pathway: a finger in every pie," *Mol. Psychiatry*, vol. 25, no. 1, pp. 131–147, Jan. 2020, doi: 10.1038/S41380-019-0414-4.

[6] K. Ishidoh, N. Kamemura, T. Imagawa, M. Oda, J. Sakurai, and N. Katunuma, "Quinolinate phosphoribosyl transferase, a key enzyme in de novo NAD+ synthesis, suppresses spontaneous cell death by inhibiting overproduction of active-caspase-3," *Biochim. Biophys. Acta - Mol. Cell Res.*, vol. 1803, no. 5, pp. 527–533, May 2010, doi: 10.1016/j.bbamcr.2010.02.007.

[7] N. Raffaelli, L. Sorci, A. Amici, M. Emanuelli, F. Mazzola, and G. Magni, "Identification of a novel human nicotinamide mononucleotide adenylyltransferase," *Biochem. Biophys. Res. Commun.*, vol. 297, no. 4, pp. 835–840, 2002, doi: 10.1016/S0006-291X(02)02285-4.

[8] Q. Han, T. Cai, D. A. Tagle, and J. Li, "Structure, expression, and function of kynurenine aminotransferases in human and rodent brains," *Cell. Mol. Life Sci.*, vol. 67, no. 3, pp. 353–368, Feb. 2010, doi: 10.1007/S00018-009-0166-4.

[9] B. Bubeck, B. Tshisuaka, S. Fetzner, and F. Lingens, "Hydroxylation of quinaldic acid: Quinaldic acid 4-monooxygenase from Alcaligenes sp. F-2 versus quinaldic acid 4-

oxidoreductases," *Biochim. Biophys. Acta - Protein Struct. Mol. Enzymol.*, vol. 1293, no. 1, pp. 39–44, Mar. 1996, doi: 10.1016/0167-4838(95)00231-6.

[10] D. Zhen, J. Liu, X. D. Zhang, and Z. Song, "Kynurenic Acid Acts as a Signaling Molecule Regulating Energy Expenditure and Is Closely Associated With Metabolic Diseases," *Front. Endocrinol. (Lausanne).*, vol. 13, Feb. 2022, doi: 10.3389/FENDO.2022.847611.

[11] Á. Szabó *et al.*, "Behavioral Balance in Tryptophan Turmoil: Regional Metabolic Rewiring in Kynurenine Aminotransferase II Knockout Mice," *Cells*, vol. 14, no. 21, Nov. 2025, doi: 10.3390/CELLS14211711.

[12] H. Jayamohanan, M. K. M. Kumar, and T. P. Aneesh, "5-HIAA as a Potential Biological Marker for Neurological and Psychiatric Disorders," *Adv. Pharm. Bull.*, vol. 9, no. 3, pp. 374–381, 2019, doi: 10.15171/APB.2019.044.

[13] R. Hardeland, "Melatonin metabolism in the central nervous system," *Curr. Neuropharmacol.*, vol. 8, no. 3, pp. 168–181, Aug. 2010, doi: 10.2174/157015910792246244.

[14] M. Berger, J. A. Gray, and B. L. Roth, "The expanded biology of serotonin," *Annu. Rev. Med.*, vol. 60, pp. 355–366, 2009, doi: 10.1146/ANNUREV.MED.60.042307.110802.

[15] E. Höglund, Ø. Øverli, and S. Winberg, "Tryptophan Metabolic Pathways and Brain Serotonergic Activity: A Comparative Review," *Front. Endocrinol. (Lausanne).*, vol. 10, no. APR, 2019, doi: 10.3389/FENDO.2019.00158.

[16] X. Ye *et al.*, "Dual Role of Indoles Derived From Intestinal Microbiota on Human Health," *Front. Immunol.*, vol. 13, Jun. 2022, doi: 10.3389/FIMMU.2022.903526/PDF.

[17] X. Su, Y. Gao, and R. Yang, "Gut Microbiota-Derived Tryptophan Metabolites Maintain Gut and Systemic Homeostasis," *Cells*, vol. 11, no. 15, Aug. 2022, doi: 10.3390/CELLS11152296.

[18] J. Gao *et al.*, "Impact of the Gut Microbiota on Intestinal Immunity Mediated by Tryptophan Metabolism," *Front. Cell. Infect. Microbiol.*, vol. 8, no. FEB, Feb. 2018, doi: 10.3389/FCIMB.2018.00013.

[19] H. S. Ranhotra, "Discrete interplay of gut microbiota L-tryptophan metabolites in host biology and disease," *Mol. Cell. Biochem.*, vol. 479, no. 9, pp. 2273–2290, Sep. 2024,

doi: 10.1007/S11010-023-04867-0.

[20] N. P. Hyland, C. R. Cavanaugh, and P. J. Hornby, “Emerging effects of tryptophan pathway metabolites and intestinal microbiota on metabolism and intestinal function,” *Amino Acids*, vol. 54, no. 1, pp. 57–70, Jan. 2022, doi: 10.1007/S00726-022-03123-X.

[21] P. Kumar, J. H. Lee, and J. Lee, “Diverse roles of microbial indole compounds in eukaryotic systems,” *Biol. Rev. Camb. Philos. Soc.*, vol. 96, no. 6, pp. 2522–2545, Dec. 2021, doi: 10.1111/BRV.12765.

[22] T. D. Hubbard, I. A. Murray, and G. H. Perdew, “Indole and Tryptophan Metabolism: Endogenous and Dietary Routes to Ah Receptor Activation,” *Drug Metab. Dispos.*, vol. 43, no. 10, pp. 1522–1535, Oct. 2015, doi: 10.1124/dmd.115.064246.

[23] D. Gao *et al.*, “DENV2 and ZIKV modulate the feeding behavior of Aedes aegypti by altering the tyrosine-dopamine pathway,” *MBio*, vol. 16, no. 6, Jun. 2025, doi: 10.1128/MBIO.03968-24.

[24] T. B. Stoker and J. C. Greenland, “Parkinson’s Disease: Pathogenesis and Clinical Aspects [Internet],” *Park. Dis. Pathog. Clin. Asp.*, pp. 1–194, Dec. 2018, doi: 10.15586/CODONPUBLICATIONS.PARKINSONSDISEASE.2018.

[25] L. Speranza, U. Di Porzio, D. Viggiano, A. de Donato, and F. Volpicelli, “Dopamine: The Neuromodulator of Long-Term Synaptic Plasticity, Reward and Movement Control,” *Cells*, vol. 10, no. 4, Apr. 2021, doi: 10.3390/CELLS10040735.

[26] M. Oakes, W. J. Law, and R. Komuniecki, “Cannabinoids Stimulate the TRP Channel-Dependent Release of Both Serotonin and Dopamine to Modulate Behavior in C. elegans,” *J. Neurosci.*, vol. 39, no. 21, pp. 4142–4152, May 2019, doi: 10.1523/JNEUROSCI.2371-18.2019.

[27] D. M. Ney *et al.*, “Metabolomic changes demonstrate reduced bioavailability of tyrosine and altered metabolism of tryptophan via the kynurenine pathway with ingestion of medical foods in phenylketonuria,” *Mol. Genet. Metab.*, vol. 121, no. 2, pp. 96–103, Jun. 2017, doi: 10.1016/j.ymgme.2017.04.003.

[28] M. Tanaka, N. Török, F. Tóth, Á. Szabó, and L. Vécsei, “Co-Players in Chronic Pain: Neuroinflammation and the Tryptophan-Kynurenine Metabolic Pathway,” *Biomedicines*, vol. 9, no. 8, Aug. 2021, doi: 10.3390/BIOMEDICINES9080897.

[29] M. Tanaka, F. Tóth, H. Polyák, Á. Szabó, Y. Mándi, and L. Vécsei, "Immune Influencers in Action: Metabolites and Enzymes of the Tryptophan-Kynurenine Metabolic Pathway," *Biomedicines*, vol. 9, no. 7, p. 734, Jun. 2021, doi: 10.3390/BIOMEDICINES9070734.

[30] M. Tanaka, Á. Szabó, E. Spekker, H. Polyák, F. Tóth, and L. Vécsei, "Mitochondrial Impairment: A Common Motif in Neuropsychiatric Presentation? The Link to the Tryptophan-Kynurenine Metabolic System," *Cells*, vol. 11, no. 16, Aug. 2022, doi: 10.3390/CELLS11162607.

[31] M. Tanaka, Á. Szabó, and L. Vécsei, "Redefining Roles: A Paradigm Shift in Tryptophan-Kynurenine Metabolism for Innovative Clinical Applications," *Int. J. Mol. Sci.*, vol. 25, no. 23, Dec. 2024, doi: 10.3390/IJMS252312767.

[32] E. Wirthgen, A. Hoeflich, A. Rebl, and J. Günther, "Kynurenic Acid: The Janus-Faced Role of an Immunomodulatory Tryptophan Metabolite and Its Link to Pathological Conditions," *Front. Immunol.*, vol. 8, no. JAN, Jan. 2018, doi: 10.3389/FIMMU.2017.01957.

[33] E. E. Abd El-Fattah, "IDO/kynurenine pathway in cancer: possible therapeutic approaches," *J. Transl. Med.*, vol. 20, no. 1, Dec. 2022, doi: 10.1186/S12967-022-03554-W.

[34] M. Ala, "The footprint of kynurenine pathway in every cancer: a new target for chemotherapy," *Eur. J. Pharmacol.*, vol. 896, Apr. 2021, doi: 10.1016/J.EJPHAR.2021.173921.

[35] M. Espi, L. Koppe, D. Fouque, and O. Thaunat, "Chronic Kidney Disease-Associated Immune Dysfunctions: Impact of Protein-Bound Uremic Retention Solutes on Immune Cells," *Toxins (Basel).*, vol. 12, no. 5, May 2020, doi: 10.3390/TOXINS12050300.

[36] D. Arnone, S. Saraykar, H. Salem, A. L. Teixeira, R. Dantzer, and S. Selvaraj, "Role of Kynurenine pathway and its metabolites in mood disorders: A systematic review and meta-analysis of clinical studies," *Neurosci. Biobehav. Rev.*, vol. 92, pp. 477–485, Sep. 2018, doi: 10.1016/J.NEUBIOREV.2018.05.031.

[37] L. Sforzini, M. A. Nettis, V. Mondelli, and C. M. Pariante, "Inflammation in cancer and depression: a starring role for the kynurenine pathway," *Psychopharmacology (Berl).*, vol. 236, no. 10, pp. 2997–3011, Oct. 2019, doi: 10.1007/S00213-019-05200-8.

[38] J. Yan *et al.*, “Molecular mechanisms and therapeutic significance of Tryptophan Metabolism and signaling in cancer,” *Mol. Cancer*, vol. 23, no. 1, Dec. 2024, doi: 10.1186/S12943-024-02164-Y.

[39] N. Török, M. Tanaka, and L. Vécsei, “Searching for peripheral biomarkers in neurodegenerative diseases: The tryptophan-kynurenine metabolic pathway,” *International Journal of Molecular Sciences*, vol. 21, no. 24. MDPI AG, pp. 1–24, Dec. 02, 2020, doi: 10.3390/ijms21249338.

[40] E. Spekker, M. Tanaka, Á. Szabó, and L. Vécsei, “Neurogenic Inflammation: The Participant in Migraine and Recent Advancements in Translational Research,” *Biomedicines*, vol. 10, no. 1, Jan. 2021, doi: 10.3390/BIOMEDICINES10010076.

[41] F. A. Boros, Z. Bohár, and L. Vécsei, “Genetic alterations affecting the genes encoding the enzymes of the kynurenine pathway and their association with human diseases,” *Mutation Research - Reviews in Mutation Research*, vol. 776. Elsevier B.V., pp. 32–45, Apr. 01, 2018, doi: 10.1016/j.mrrev.2018.03.001.

[42] R. Kearns, “The Kynurenine Pathway in Gut Permeability and Inflammation,” *Inflammation*, vol. 48, no. 3, pp. 1063–1077, Jun. 2025, doi: 10.1007/S10753-024-02135-X.

[43] H. Polyák *et al.*, “Cuprizone markedly decreases kynurenic acid levels in the rodent brain tissue and plasma,” *Heliyon*, vol. 7, no. 2, Feb. 2021, doi: 10.1016/J.HELIYON.2021.E06124.

[44] H. Polyák *et al.*, “The Tryptophan-Kynurenine Metabolic System Is Suppressed in Cuprizone-Induced Model of Demyelination Simulating Progressive Multiple Sclerosis,” *Biomedicines*, vol. 11, no. 3, Mar. 2023, doi: 10.3390/BIOMEDICINES11030945.

[45] A. Johri and M. F. Beal, “Alzheimer’s disease: Recent concepts on the relation of mitochondrial disturbances, excitotoxicity, neuroinflammation, and kynurenines,” *Journal of Pharmacology and Experimental Therapeutics*. 2012, doi: 10.1124/jpet.112.192138.

[46] G. Mazarei and B. R. Leavitt, “Indoleamine 2,3 Dioxygenase as a Potential Therapeutic Target in Huntington’s Disease,” *J. Huntingtons. Dis.*, vol. 4, no. 2, pp. 109–118, Jul. 2015, doi: 10.3233/JHD-159003.

[47] C. K. Lim *et al.*, "Involvement of the kynurenine pathway in the pathogenesis of Parkinson's disease," *Prog. Neurobiol.*, vol. 155, pp. 76–95, Aug. 2017, doi: 10.1016/J.PNEUROBIO.2015.12.009.

[48] M. Tanaka, E. Spekker, Á. Szabó, H. Polyák, and L. Vécsei, "Modelling the neurodevelopmental pathogenesis in neuropsychiatric disorders. Bioactive kynurenines and their analogues as neuroprotective agents-in celebration of 80th birthday of Professor Peter Riederer," *J. Neural Transm.*, vol. 129, no. 5–6, pp. 627–642, Jun. 2022, doi: 10.1007/S00702-022-02513-5.

[49] A. Muneer, "Kynurenine Pathway of Tryptophan Metabolism in Neuropsychiatric Disorders: Pathophysiologic and Therapeutic Considerations," *Clin. Psychopharmacol. Neurosci.*, vol. 18, no. 4, pp. 507–526, Nov. 2020, doi: 10.9758/CPN.2020.18.4.507.

[50] J. de Bie, C. K. Lim, and G. J. Guillemin, "Kynurenines, Gender and Neuroinflammation; Showcase Schizophrenia," *Neurotox. Res.*, vol. 30, no. 3, pp. 285–294, Oct. 2016, doi: 10.1007/S12640-016-9641-5.

[51] R. Machado-Vieira and C. A. Zarate, "Proof of concept trials in bipolar disorder and major depressive disorder: a translational perspective in the search for improved treatments," *Depress. Anxiety*, vol. 28, no. 4, pp. 267–281, Apr. 2011, doi: 10.1002/DA.20800.

[52] M. Tanaka and G. Telegdy, "Involvement of adrenergic and serotonergic receptors in antidepressant-like effect of urocortin 3 in a modified forced swimming test in mice," *Brain Res. Bull.*, vol. 77, no. 5, pp. 301–305, Nov. 2008, doi: 10.1016/j.brainresbull.2008.08.012.

[53] M. Tanaka, A. V. Schally, and G. Telegdy, "Neurotransmission of the antidepressant-like effects of the growth hormone-releasing hormone antagonist MZ-4-71," *Behav. Brain Res.*, vol. 228, no. 2, pp. 388–391, Mar. 2012, doi: 10.1016/j.bbr.2011.12.022.

[54] T. Kaiser and G. Feng, "Modeling psychiatric disorders for developing effective treatments," *Nat. Med.*, vol. 21, no. 9, pp. 979–988, Sep. 2015, doi: 10.1038/NM.3935.

[55] M. T. Pan, H. Zhang, X. J. Li, and X. Y. Guo, "Genetically modified non-human primate models for research on neurodegenerative diseases," *Zool. Res.*, vol. 45, no. 2, pp. 263–274, 2024, doi: 10.24272/J.ISSN.2095-8137.2023.197.

[56] X. J. Li and W. Li, “Beyond Mice: Genetically Modifying Larger Animals to Model Human Diseases,” *J. Genet. Genomics*, vol. 39, no. 6, pp. 237–238, Jun. 2012, doi: 10.1016/j.jgg.2012.05.006.

[57] I. E. Holm, A. K. O. Alstrup, and Y. Luo, “Genetically modified pig models for neurodegenerative disorders,” *J. Pathol.*, vol. 238, no. 2, pp. 267–287, Jan. 2016, doi: 10.1002/PATH.4654.

[58] P. Yu *et al.*, “Biochemical and phenotypic abnormalities in kynurenine aminotransferase II-deficient mice,” *Mol. Cell. Biol.*, vol. 24, no. 16, pp. 6919–6930, Aug. 2004, doi: 10.1128/MCB.24.16.6919-6930.2004.

[59] P. Yu, Z. Li, L. Zhang, D. A. Tagle, and T. Cai, “Characterization of kynurenine aminotransferase III, a novel member of a phylogenetically conserved KAT family,” *Gene*, vol. 365, no. 1-2 SPEC. ISS., pp. 111–118, Jan. 2006, doi: 10.1016/j.gene.2005.09.034.

[60] F. M. Notarangelo, S. Beggiato, and R. Schwarcz, “Assessment of Prenatal Kynurenine Metabolism Using Tissue Slices: Focus on the Neosynthesis of Kynurenic Acid in Mice,” *Dev. Neurosci.*, vol. 41, no. 1–2, pp. 102–111, Sep. 2019, doi: 10.1159/000499736.

[61] M. C. Potter *et al.*, “Reduction of endogenous kynurenic acid formation enhances extracellular glutamate, hippocampal plasticity, and cognitive behavior,” *Neuropsychopharmacology*, vol. 35, no. 8, pp. 1734–1742, Jul. 2010, doi: 10.1038/NPP.2010.39.

[62] S. Erhardt *et al.*, “Adaptive and Behavioral Changes in Kynurenine 3-Monooxygenase Knockout Mice: Relevance to Psychotic Disorders,” *Biol. Psychiatry*, vol. 82, no. 10, pp. 756–765, Nov. 2017, doi: 10.1016/j.biopsych.2016.12.011.

[63] T. Tashiro *et al.*, “Kynurenine 3-monooxygenase is implicated in antidepressants-responsive depressive-like behaviors and monoaminergic dysfunctions,” *Behav. Brain Res.*, vol. 317, pp. 279–285, Jan. 2017, doi: 10.1016/j.bbr.2016.09.050.

[64] V. Choudhary *et al.*, “Loss of Indoleamine-2,3-Dioxygenase-1 (IDO1) in Knockout Mice Does Not Affect the Development of Skin Lesions in the Imiquimod-Induced Mouse Model of Psoriasis,” *Int. J. Tryptophan Res.*, vol. 15, Feb. 2022, doi: 10.1177/11786469221078191.

[65] A. G. Aslamkhan *et al.*, "Characterization of indoleamine-2,3-dioxygenase 1, tryptophan-2,3-dioxygenase, and Ido1/Tdo2 knockout mice," *Toxicol. Appl. Pharmacol.*, vol. 406, Nov. 2020, doi: 10.1016/j.taap.2020.115216.

[66] L. Vécsei, L. Szalárdy, F. Fülöp, and J. Toldi, "Kynurenines in the CNS: Recent advances and new questions," *Nature Reviews Drug Discovery*, vol. 12, no. 1. Nat Rev Drug Discov, pp. 64–82, Jan. 2013, doi: 10.1038/nrd3793.

[67] P. D. Leeson *et al.*, "Kynurenic acid derivatives. Structure-activity relationships for excitatory amino acid antagonism and identification of potent and selective antagonists at the glycine site on the N-methyl-D-aspartate receptor," *J. Med. Chem.*, vol. 34, no. 4, pp. 1243–1252, Apr. 1991, doi: 10.1021/JM00108A002.

[68] É. Rózsa, H. Robotka, L. Vécsei, and J. Toldi, "The Janus-face kynurenic acid," *J. Neural Transm.*, vol. 115, no. 8, pp. 1087–1091, Aug. 2008, doi: 10.1007/s00702-008-0052-5.

[69] Á. Szabó *et al.*, "Oxidative and Excitatory Neurotoxic Stresses in CRISPR/Cas9-Induced Kynurenine Aminotransferase Knockout Mice: A Novel Model for Despair-Based Depression and Post-Traumatic Stress Disorder," *Front. Biosci. (Landmark Ed.*, vol. 30, no. 1, Jan. 2025, doi: 10.31083/FBL25706.

[70] G. E. Truett, P. Heeger, R. L. Mynatt, A. A. Truett, J. A. Walker, and M. L. Warman, "Preparation of PCR-quality mouse genomic DNA with hot sodium hydroxide and tris (HotSHOT)," *Biotechniques*, vol. 29, no. 1, pp. 52–54, 2000, doi: 10.2144/00291BM09.

[71] Z. Galla *et al.*, "Simultaneous determination of 30 neurologically and metabolically important molecules: A sensitive and selective way to measure tyrosine and tryptophan pathway metabolites and other biomarkers in human serum and cerebrospinal fluid," *J. Chromatogr. A*, vol. 1635, Jan. 2021, doi: 10.1016/j.chroma.2020.461775.

[72] Z. Galla *et al.*, "Improved LC-MS/MS method for the determination of 42 neurologically and metabolically important molecules in urine," *J. Chromatogr. B Anal. Technol. Biomed. Life Sci.*, vol. 1179, Aug. 2021, doi: 10.1016/j.jchromb.2021.122846.

[73] A. A. B. Badawy, "Kynurenine pathway of tryptophan metabolism: Regulatory and functional aspects," *International Journal of Tryptophan Research*, vol. 10, no. 1. SAGE Publications Ltd, 2017, doi: 10.1177/1178646917691938.

[74] D. A. Bender, "Biochemistry of tryptophan in health and disease," *Mol. Aspects Med.*, vol. 6, no. 2, pp. 101–197, 1983, doi: 10.1016/0098-2997(83)90005-5.

[75] R. Schwarcz, J. P. Bruno, P. J. Muchowski, and H. Q. Wu, "Kynurenines in the mammalian brain: when physiology meets pathology," *Nat. Rev. Neurosci.*, vol. 13, no. 7, pp. 465–477, Jul. 2012, doi: 10.1038/NRN3257.

[76] I. Wonodi and R. Schwarcz, "Cortical kynurenine pathway metabolism: a novel target for cognitive enhancement in Schizophrenia," *Schizophr. Bull.*, vol. 36, no. 2, pp. 211–218, Mar. 2010, doi: 10.1093/SCHBUL/SBQ002.

[77] M. Hamon and J. Glowinski, "Regulation of serotonin synthesis," *Life Sci.*, vol. 15, no. 9, pp. 1533–1548, Nov. 1974, doi: 10.1016/0024-3205(74)90320-8.

[78] E. Kabadayi Sahin, A. Caykoylu, A. Senat, and O. Erel, "A comprehensive study of oxidative stress in patients with somatic symptom disorder," *Acta Neuropsychiatr.*, vol. 31, no. 2, pp. 100–105, Apr. 2019, doi: 10.1017/NEU.2018.33.

[79] N. Polat, H. Beyaztas, S. Aktas, O. Maden, and E. Metin Guler, "Comparison of oxidative stress parameters, thiol-disulfide homeostasis, and pro-inflammatory cytokines levels in patients with bipolar disorder and their first-degree relatives," *J. Psychiatr. Res.*, vol. 162, pp. 103–112, Jun. 2023, doi: 10.1016/j.jpsychires.2023.05.022.

[80] D. Juchnowicz *et al.*, "Oxidative Stress Biomarkers as a Predictor of Stage Illness and Clinical Course of Schizophrenia," *Front. psychiatry*, vol. 12, Nov. 2021, doi: 10.3389/FPSYT.2021.728986.

[81] P. Barone, "The 'Yin' and the 'Yang' of the kynurenine pathway: excitotoxicity and neuroprotection imbalance in stress-induced disorders," *Behav. Pharmacol.*, vol. 30, no. 2 and 3-Spec Issue, pp. 163–186, Apr. 2019, doi: 10.1097/FBP.0000000000000477.

[82] M. Y. T. Globus, M. D. Ginsberg, and R. Busto, "Excitotoxic index - a biochemical marker of selective vulnerability," *Neurosci. Lett.*, vol. 127, no. 1, pp. 39–42, Jun. 1991, doi: 10.1016/0304-3940(91)90889-2.

[83] D. C. Rogers *et al.*, "SHIRPA, a protocol for behavioral assessment: Validation for longitudinal study of neurological dysfunction in mice," *Neurosci. Lett.*, vol. 306, no. 1–2, pp. 89–92, Jun. 2001, doi: 10.1016/S0304-3940(01)01885-7.

[84] R. Lalonde, M. Filali, and C. Strazielle, "SHIRPA as a Neurological Screening Battery

in Mice," *Curr. Protoc.*, vol. 1, no. 5, May 2021, doi: 10.1002/CPZ1.135.

[85] D. C. Rogers, E. M. C. Fisher, S. D. M. Brown, J. Peters, A. J. Hunter, and J. E. Martin, "Behavioral and functional analysis of mouse phenotype: SHIRPA, a proposed protocol for comprehensive phenotype assessment," *Mamm. Genome*, vol. 8, no. 10, pp. 711–713, 1997, doi: 10.1007/S003359900551.

[86] A. K. Kraeuter, P. C. Guest, and Z. Sarnyai, "The Open Field Test for Measuring Locomotor Activity and Anxiety-Like Behavior," *Methods Mol. Biol.*, vol. 1916, pp. 99–103, 2019, doi: 10.1007/978-1-4939-8994-2_9.

[87] S. C. Stanford, "The Open Field Test: reinventing the wheel," *J. Psychopharmacol.*, vol. 21, no. 2, pp. 134–135, Mar. 2007, doi: 10.1177/0269881107073199.

[88] C. Lubrich, P. Giesler, and M. Kipp, "Motor Behavioral Deficits in the Cuprizone Model: Validity of the Rotarod Test Paradigm," *Int. J. Mol. Sci.*, vol. 23, no. 19, Oct. 2022, doi: 10.3390/IJMS231911342.

[89] H. M. Shan, M. A. Maurer, and M. E. Schwab, "Four-parameter analysis in modified Rotarod test for detecting minor motor deficits in mice," *BMC Biol.*, vol. 21, no. 1, Dec. 2023, doi: 10.1186/S12915-023-01679-Y.

[90] J. H. Widjaja, D. C. Sloan, J. A. Hauger, and B. S. Muntean, "Customizable Open-Source Rotating Rod (Rotarod) Enables Robust Low-Cost Assessment of Motor Performance in Mice," *eNeuro*, vol. 10, no. 9, Sep. 2023, doi: 10.1523/ENEURO.0123-23.2023.

[91] S. P. Keane, K. K. Chadman, A. R. Gomez, and W. Hu, "Pros and cons of narrow- versus wide-compartment rotarod apparatus: An experimental study in mice," *Behav. Brain Res.*, vol. 463, Apr. 2024, doi: 10.1016/j.bbr.2024.114901.

[92] R. G. Lister, "The use of a plus-maze to measure anxiety in the mouse," *Psychopharmacology (Berl).*, vol. 92, no. 2, pp. 180–185, Jun. 1987, doi: 10.1007/BF00177912.

[93] S. Pellow, P. Chopin, S. E. File, and M. Briley, "Validation of open:closed arm entries in an elevated plus-maze as a measure of anxiety in the rat," *J. Neurosci. Methods*, vol. 14, no. 3, pp. 149–167, 1985, doi: 10.1016/0165-0270(85)90031-7.

[94] E. S. Onaivi and B. R. Martin, "Neuropharmacological and physiological validation of a computer-controlled two-compartment black and white box for the assessment of

anxiety," *Prog. Neuropsychopharmacol. Biol. Psychiatry*, vol. 13, no. 6, 1989, doi: 10.1016/0278-5846(89)90047-X.

[95] M. Bourin and M. Hascoët, "The mouse light/dark box test," *Eur. J. Pharmacol.*, vol. 463, no. 1–3, pp. 55–65, Feb. 2003, doi: 10.1016/S0014-2999(03)01274-3.

[96] S. N. Narayanan and R. S. Kumar, "An improved light dark box test by using a real-time video tracking system," *Acta Biol. Hung.*, vol. 69, no. 4, pp. 371–384, Dec. 2018, doi: 10.1556/018.69.2018.4.1.

[97] M. J. Detke, M. Rickels, and I. Lucki, "Active behaviors in the rat forced swimming test differentially produced by serotonergic and noradrenergic antidepressants," *Psychopharmacology (Berl).*, vol. 121, no. 1, pp. 66–72, Sep. 1995, doi: 10.1007/BF02245592.

[98] R. T. Khisti, C. T. Chopde, and S. P. Jain, "Antidepressant-like effect of the neurosteroid 3alpha-hydroxy-5alpha-pregnan-20-one in mice forced swim test," *Pharmacol. Biochem. Behav.*, vol. 67, no. 1, pp. 137–143, 2000, doi: 10.1016/S0091-3057(00)00300-2.

[99] M. Tanaka, Z. Bohár, D. Martos, G. Telegdy, and L. Vécsei, "Antidepressant-like effects of kynurenic acid in a modified forced swim test," *Pharmacol. Reports*, vol. 72, no. 2, pp. 449–455, Apr. 2020, doi: 10.1007/s43440-020-00067-5.

[100] L. Steru, R. Chermat, B. Thierry, and P. Simon, "The tail suspension test: a new method for screening antidepressants in mice," *Psychopharmacology (Berl).*, vol. 85, no. 3, pp. 367–370, Mar. 1985, doi: 10.1007/BF00428203.

[101] J. F. Cryan, C. Mombereau, and A. Vassout, "The tail suspension test as a model for assessing antidepressant activity: Review of pharmacological and genetic studies in mice," *Neurosci. Biobehav. Rev.*, vol. 29, no. 4–5, pp. 571–625, 2005, doi: 10.1016/j.neubiorev.2005.03.009.

[102] F. Muntoni, A. Mateddu, and G. Serra, "Passive avoidance behaviour deficit in the mdx mouse," *Neuromuscul. Disord.*, vol. 1, no. 2, pp. 121–123, 1991, doi: 10.1016/0960-8966(91)90059-2.

[103] V. R. Ostovan, Z. Amiri, L. Moezi, F. Pirsalami, Z. Esmaili, and M. Moosavi, "The effects of subchronic agmatine on passive avoidance memory, anxiety-like behavior and

hippocampal Akt/GSK-3β in mice," *Behav. Pharmacol.*, vol. 33, no. 1, pp. 42–50, Feb. 2022, doi: 10.1097/FBP.0000000000000666.

[104] M. Kruk-Slomka and G. Biala, "Cannabidiol Attenuates MK-801-Induced Cognitive Symptoms of Schizophrenia in the Passive Avoidance Test in Mice," *Molecules*, vol. 26, no. 19, Oct. 2021, doi: 10.3390/MOLECULES26195977.

[105] L. M. Lueptow, "Novel Object Recognition Test for the Investigation of Learning and Memory in Mice," *J. Vis. Exp.*, vol. 2017, no. 126, Aug. 2017, doi: 10.3791/55718.

[106] B. Grayson, M. Leger, C. Piercy, L. Adamson, M. Harte, and J. C. Neill, "Assessment of disease-related cognitive impairments using the novel object recognition (NOR) task in rodents," *Behav. Brain Res.*, vol. 285, pp. 176–193, May 2015, doi: 10.1016/j.bbr.2014.10.025.

[107] S. J. Cohen and R. W. Stackman, "Assessing rodent hippocampal involvement in the novel object recognition task. A review," *Behav. Brain Res.*, vol. 285, pp. 105–117, May 2015, doi: 10.1016/j.bbr.2014.08.002.

[108] J. K. Denninger, B. M. Smith, and E. D. Kirby, "Novel Object Recognition and Object Location Behavioral Testing in Mice on a Budget," *J. Vis. Exp.*, vol. 2018, no. 141, Nov. 2018, doi: 10.3791/58593.

[109] B. Wulaer *et al.*, "Prefrontal cortex, dorsomedial striatum, and dentate gyrus are necessary in the object-based attention test in mice," *Mol. Brain*, vol. 13, no. 1, Dec. 2020, doi: 10.1186/S13041-020-00711-4.

[110] B. Wulaer *et al.*, "Pharmacological blockade of dopamine D1- or D2-receptor in the prefrontal cortex induces attentional impairment in the object-based attention test through different neuronal circuits in mice," *Mol. Brain*, vol. 14, no. 1, Dec. 2021, doi: 10.1186/S13041-021-00760-3.

[111] G. Věchetová *et al.*, "Attention impairment in motor functional neurological disorders: a neuropsychological study," *J. Neurol.*, vol. 269, no. 11, pp. 5981–5990, Nov. 2022, doi: 10.1007/S00415-022-11211-X.

[112] T. Yoon, J. Okada, M. W. Jung, and J. J. Kim, "Prefrontal cortex and hippocampus subserve different components of working memory in rats," *Learn. Mem.*, vol. 15, no. 3, pp. 97–105, Mar. 2008, doi: 10.1101/LM.850808.

[113] A. K. Kraeuter, P. C. Guest, and Z. Sarnyai, "The Y-Maze for Assessment of Spatial Working and Reference Memory in Mice," *Methods Mol. Biol.*, vol. 1916, pp. 105–111, 2019, doi: 10.1007/978-1-4939-8994-2_10.

[114] E. A. K. Prieur and N. M. Jadavji, "Assessing Spatial Working Memory Using the Spontaneous Alternation Y-maze Test in Aged Male Mice," *Bio-protocol*, vol. 9, no. 3, Feb. 2019, doi: 10.21769/BIOPROTOC.3162.

[115] P. V. Dixit, R. Sahu, and D. K. Mishra, "Marble-burying behavior test as a murine model of compulsive-like behavior," *J. Pharmacol. Toxicol. Methods*, vol. 102, Mar. 2020, doi: 10.1016/j.vascn.2020.106676.

[116] A. Thomas, A. Burant, N. Bui, D. Graham, L. A. Yuva-Paylor, and R. Paylor, "Marble burying reflects a repetitive and perseverative behavior more than novelty-induced anxiety," *Psychopharmacology (Berl).*, vol. 204, no. 2, pp. 361–373, Jun. 2009, doi: 10.1007/S00213-009-1466-Y.

[117] G. de Brouwer and D. W. Wolmarans, "Back to basics: A methodological perspective on marble-burying behavior as a screening test for psychiatric illness," *Behav. Processes*, vol. 157, pp. 590–600, Dec. 2018, doi: 10.1016/j.beproc.2018.04.011.

[118] E. Langer, H. Einat, and Y. Stukalin, "Similarities and dissimilarities in the effects of benzodiazepines and specific serotonin reuptake inhibitors (SSRIs) in the defensive marble burying test: A systematic review and meta-analysis," *Eur. Neuropsychopharmacol.*, vol. 36, pp. 38–49, Jul. 2020, doi: 10.1016/j.euroneuro.2020.04.007.

[119] M. Yang, J. L. Silverman, and J. N. Crawley, "Automated three-chambered social approach task for mice," *Curr. Protoc. Neurosci.*, vol. Chapter 8, no. SUPPL. 56, 2011, doi: 10.1002/0471142301.NS0826S56.

[120] L. D. Oliver, I. Moxon-Emre, M. C. Lai, L. Grennan, A. N. Voineskos, and S. H. Ameis, "Social Cognitive Performance in Schizophrenia Spectrum Disorders Compared With Autism Spectrum Disorder: A Systematic Review, Meta-analysis, and Meta-regression," *JAMA psychiatry*, vol. 78, no. 3, pp. 281–292, Mar. 2021, doi: 10.1001/JAMAPSYCHIATRY.2020.3908.

[121] J. M. Fernandes, R. Cajão, R. Lopes, R. Jerónimo, and J. B. Barahona-Corrêa, "Social Cognition in Schizophrenia and Autism Spectrum Disorders: A Systematic Review and

Meta-Analysis of Direct Comparisons," *Front. psychiatry*, vol. 9, Oct. 2018, doi: 10.3389/FPSYT.2018.00504.

[122] A. E. Pinkham *et al.*, "Comprehensive comparison of social cognitive performance in autism spectrum disorder and schizophrenia," *Psychol. Med.*, vol. 50, no. 15, pp. 2557–2565, Nov. 2020, doi: 10.1017/S0033291719002708.

[123] H. Arakawa, "Revisiting sociability: Factors facilitating approach and avoidance during the three-chamber test," *Physiol. Behav.*, vol. 272, Dec. 2023, doi: 10.1016/j.physbeh.2023.114373.